

Article

# Adaptive Rejection of a Sinusoidal Disturbance with Unknown Frequency in a Flexible Rotor with Lubricated Journal Bearings

Gerardo Amato <sup>1</sup>, Roberto D'Amato <sup>2,3,\*</sup> and Alessandro Ruggiero <sup>4</sup>

- <sup>1</sup> Nonlinear and Adaptive Controls Laboratory, Department of Electronic Engineering, University of Rome "Tor Vergata", Via del Politecnico, 00133 Rome, Italy; amato@ing.uniroma2.it
- <sup>2</sup> Escuela Técnica Superior de Ingeniería y Diseño Industrial, Universidad Politécnica de Madrid, Ronda de Valencia, 28012 Madrid, Spain
- <sup>3</sup> Structural Materials Research Center (CIME-UPM), Departamento de Ciencia de Materiales ETS de Ingenieros de Caminos, Canales y Puertos, C/Profesor Aranguren S/N, 28040 Madrid, Spain
- <sup>4</sup> Department of Industrial Engineering, University of Salerno, Via Giovanni Paolo II, 84084 Fisciano, Italy; ruggiero@unisa.it
- \* Correspondence: r.damato@upm.es

**Abstract:** Frequency-dependent adaptive noise cancellation-based tracking controller (ANC-TC) is a known technique for the stabilization of several nonlinear dynamical systems. In recent years, this control strategy has been introduced and applied for the stabilization of a flexible rotor supported on full-lubricated journal bearings. This paper proposes a theoretical investigation, based on robust immersion and invariance (I&I) theory, of a novel ANC-frequency estimation (FE) technique designed to stabilize a flexible rotor shaft affected by self-generated sinusoidal disturbances, generalized to the case of unknown frequency. A structural proof, under assumptions on closed-loop output signals, shows that the sinusoidal disturbance rejection is exponential. Numerical simulations are presented to validate the mathematical results in silico. The iterative Inexact Newton method is applied to the disturbance frequency and phase estimation error point series. The data fitting confirms that the phase estimation succession has an exponential convergence behavior and that the asymptotical frequency estimation is a warm-up phase of the overall close-loop disturbance estimation process. In two different operating conditions, the orders of convergence obtained by phase and frequency estimate timeseries are  $p_\varphi = 1$ ,  $p_{\omega,unc} = 0.9983$  and  $p_{\omega,cav} = 1.005$ . Rejection of the rotor dynamic disturbance occurs approximately 76% before in the cavitated than in the uncavitated condition, 2 (s) and 8.5 (s), respectively.

**Keywords:** rotordynamic; adaptive rejection control; sinusoidal disturbance; flexible rotor; hydrodynamic journal bearing

**MSC:** 37M05; 37N35



**Citation:** Amato, G.; D'Amato, R.; Ruggiero, A. Adaptive Rejection of a Sinusoidal Disturbance with Unknown Frequency in a Flexible Rotor with Lubricated Journal Bearings. *Mathematics* **2022**, *10*, 1703. <https://doi.org/10.3390/math10101703>

Academic Editors: Higinio Rubio Alonso, Alejandro Bustos Caballero, Jesus Meneses Alonso and Enrique Soriano-Heras

Received: 15 April 2022

Accepted: 10 May 2022

Published: 16 May 2022

**Publisher's Note:** MDPI stays neutral with regard to jurisdictional claims in published maps and institutional affiliations.



**Copyright:** © 2022 by the authors. Licensee MDPI, Basel, Switzerland. This article is an open access article distributed under the terms and conditions of the Creative Commons Attribution (CC BY) license (<https://creativecommons.org/licenses/by/4.0/>).

## 1. Introduction

### 1.1. Problem Statement: Flexible Rotor with Lubricated Journal Bearings

In rotating machines, bearings are used to transfer radial and axial forces in a supporting structure ensuring a low value of the coefficient of friction and good system stability [1,2]. For cases with high loads and high rotational speeds, fluid film lubricated bearings are often preferred. The latter can be of two main categories: hydrodynamic bearings and hydrostatic bearings [3]. In the case of hydrodynamic bearings, the relative movement between the two coupled surfaces (journal and bearing) generates a pressurized fluid film that reduces the friction forces, ensuring the necessary support for the external load [3]. In the case of hydrostatic bearings, the pressure of the lubricating fluid is guaranteed by the action of an external pump, which injects pressurized lubricant into the bearing [4]. The most common version of hydrodynamic bearings is the full journal bearing,

which consists of a rotor (journal) that rotates inside a bearing with a diameter slightly larger than that of the rotor, and the fluid film exists in the small space between the two (meatus) [3]. In the unsteady dynamical behavior, fluid film bearings can, however, present oscillating behavior (typical elliptical orbits) due to destabilizing cross coupling forces caused by the nonlinear fluid dynamic phenomena in the oil film [2,5]. To obtain acceptable operating conditions, it is necessary to simultaneously analyze the rotor-journal bearing couple in the case of a flexible rotor. These types of dynamic systems exhibit a particular type of self-excited vibration due to fluid dynamics phenomena in the oil film [2] known as *oil whirl* and *oil whip*, and are characterized by subsynchronous processional motions [6,7]. These vibrations appear when the subsynchronous vortex frequency reaches the natural frequency of the system [8] and is typically characterized by high vibration amplitudes. In recent years, research has shown that oil whirl phenomena are generated also when the journal bearing runs on micropolar lubricant [9–11]. Many authors have studied the effect of lubricant contamination [12] and the nonlinear behavior of film-oil main bearings in rotating machines [13]. Furthermore, the performance of the bearing, in order to avoid instability phenomena, has been analyzed, studied and simulated considering factors such as misalignment [14], elasticity of the bearing liner [15], dynamic conditions and coupled surface roughness [16].

### 1.2. Literary Review: Active Noise Rejection Control

One of the objectives of recent research has been to propose control strategies for solving the classical problem of vibration rejection, in the frame of flexible mechanical structures [17,18], flexible rotor bearings control [19–23] and their active balancing [21]. The aim is to absorb, or reject, any vibrational phenomena on a rotating shaft connected to a motor, and stabilize it around an arbitrary equilibrium position [24], for example, using a closed-loop controller with notch filtering actions [24–26]. Good attenuation features are obtained if the disturbance frequency is well-known. Indeed, the stop bands of these filtering-based controllers exhibit very steep edges. Usually, in the presence of unmodelled dynamics, observer-based and sliding mode observer-based controls allow for the tracking control precision to be improved by adapting to the unmatched uncertainties [18]. Nevertheless, the use of an adaptive observer to solve this category of problems, the vibration suppression in flexible mechanical system, is not so widespread. For example [26], avoids the application of an adaptive observer due to the risk of control spillover. Conversely, the ANC control in D’Amato et al. [24] is implemented as an observer-based control. In [24], the equations of the elastic contributions in the journal bearings and the relative vibrations are modelled as a separated exosystem [27], which represents the disturbance acting on the control. Then, the ANC operation consists of the observation of such disturbance elastic contributions, so that the control injects, on purpose, a counterphase oscillation, aiming to delete them. This makes the closed-loop control independent of the operating conditions of the bearings: cavitated and uncavitating.

First results concerning controllability and observability problems in rotordynamic systems date back to the 1980s. The flexible rotor and the flexibly-mounted journal bearings were modelled by Stanway and Burrows, 1981 [22], as a spring-damping-mass system, with well-known natural vibration modes. They determined the system observability and controllability conditions in order to assign directly the closed-loop eigenvalues with a linear controller. A linear control approach was also addressed by Lei and Palazzolo, 2008 [25]. To this aim they used the Finite-Element-Method (FEM) to model the rotor dynamic system. In their approach, active magnetic bearings (AMB) were employed to handle the rotordynamic systems by acting coaxially to the inertial axis through a linear control law. In the framework of control techniques which uses AMB, Kumar and Tiwari, 2020 [28], investigated the rotordynamic system modeling unbalance and misalignment with the rigid body theory. The possibility of modeling the flexible system with a new set of nonlinear closed-form equations is a definite novelty introduced by D’Amato et al., 2022 [24], and retrieved in this presented study. By considering the lubricated bearing

dynamic effects and with lubricant film cavitation conditions, an input–output feedback linearizing controller can be implemented. The proposed control law is adaptive with respect to the control and disturbance parameter (i.e., phase and frequency of the sinusoidal disturbance, corresponding to rotor angular speed of the rotor).

### 1.3. Proposed Control Strategy: ANC with Frequency Estimation

This paper proposes a theoretical investigation of a novel ANC-frequency estimation (FE) technique designed to stabilize a flexible rotor shaft affected by self-generated sinusoidal disturbances. This work extends the adaptive noise cancellation tracking control (ANC-TC) algorithm presented by D’Amato et al. in 2022 [24,29], generalized to the case of unknown frequency. The disturbance frequency corresponds to the rotor operating angular speed ( $\omega$ ) [20,24,30], which is driven by an external actuator, so that uncertainties may arise in the frequency actual value due to actuation operating point fluctuations. Other incoming nonlinear phenomena, such as gyroscopic moments acting on the disk—for example due to asymmetries of the rotor support [31]—can make the operating frequency vary. The ANC-TC in [24,29] uses such a frequency value as a known parameter, which is also a parameter of the dynamics of the system. With respect to the specific uncavitated case study [29], a theoretical formulation has been provided in [24]: structural proofs for noise suppression estimation, cancellation and system stabilization are given when the disturbance frequency is known but not the initial condition. In this paper, inspired by immersion and invariance (I&I) robust control techniques [18,32,33], the possibility of estimating online the constant unknown frequency of the disturbance is considered. Following I&I-based approaches, the studied controlled system is immersed into a target dynamical model so that its trajectories are an image of the target dynamic system into the immersion map. Then, the aim of this kind of approach is to make the target system image an attractive manifold, so that the controlled system is made globally, uniformly, asymptotically stable around its invariant trajectories [18,32,33].

The approach of [33] was convoluted in the hybrid logic (even if in a more general sense with respect to [32]). The general multi-harmonic disturbance case may be considered [17,33]. An I&I-based strategy, adaptive with respect to perturbation parameters, was recently presented and applied to a reversible cold strip rolling mill to control the speed and tension system [18], characterized by severe coupling effects, multiple state-variables, nonlinearities and model uncertainties. In [18], it was shown that the estimation errors follow an exponential convergence.

A recent research work [17] deals with the problem of active multi-harmonic disturbances cancellation in flexible mechanical structures, under the analysis of passivity properties of a closed-loop system. The controller operates an inner loop, which performs the position control of the system, while the frequency estimation is demanded to an outer control loop, elaborating the position measurements of the plant. A robust linear compensator scheme, non-accurate model-based, was employed and experimentally validated. An exponential cancellation of the disturbance was obtained.

The ANC-TC in [24,29] already showed an intrinsic robustness since the vibrational disturbances acting on the rotor were cancelled. Consequently, the introduction of a frequency identifier for vibrational modes improves the robustness of the method.

The closed-loop sinusoidal noise rejection is conceived in two phases: first, the operating frequency identification is performed as a combination of state-observer and asymptotical parameter estimation [32,33]; second, the asymptotical frequency estimate is fed back to the closed-loop adaptive noise cancellation control (ANC), which hooks the phase of the disturbance by injecting on rotor dynamics a counterphase sinusoid acceleration. The frequency estimation is in practice a warm-up phase of the overall closed-loop control [34,35]. This study proposed a unified theoretical structure including an I&I-based frequency estimator as a plug-in control block. The proposed control architecture design concerns the externalization of the FE process, which appears as an additive standalone block downstream to the ANC closed-loop, elaborating its output data and generating the

asymptotical frequency estimate. Once such an asymptotical estimate converges at the steady-state closed-loop, the ANC control exponentially hooks the sinusoidal disturbance, following [24].

Table 1 itemizes and catalogues the scientific literary references that are investigated as background for the proposed study.

**Table 1.** Literary review.

Authors	Year	Source	Section Content	Authors	Year	Source	Section Content
Poritsky	1953	[8]	PS	Avramov and Borysiuk	2012	[31]	PCS
Stanway and Burrows	1981	[22]	LR	Harika et al.	2013	[12]	PS
Burrows and Sahinkaya	1983	[19]	LR	Marino and Tomei	2016	[27]	LR
Lund	1987	[2]	PS	Carnevale	2016	[33]	PCS
Vance	1988	[30]	PCS	Salazar and Santos	2017	[4]	PS
Muszynska	1988	[6]	PS	Zheng et al.	2017	[23]	LR
D’Agostno et al.	2001	[7]	PS	Ruggiero et al.	2018	[20]	LR, PCS
Zhou and Shi	2001	[21]	LR	Ballnus et al.	2018	[35]	PCS
Hamrock and Schmid	2004	[3]	PS	Das and Guha	2019	[10]	PS
Sukumaran Nair and Prabhakaran	2004	[15]	PS	Bhattacharjee et al.	2019	[11]	PS
Das et al.	2005	[14]	PS	D’Amato et al.	2019	[29]	PCS
Ypma	2006	[36]	PCS	Marko et al.	2020	[26]	LR
Prabhakaran Nair et al.	2007	[16]	PS	Kumar and Tiwari	2020	[28]	LR
Lei and Palazzolo	2008	[25]	LR	Chen et al.	2021	[5]	PS
Carnevale and Astolfi	2008	[32]	PCS	Tripathy and Bhattacharyya	2022	[9]	PS
Friswell et al.	2010	[1]	PS	Liu et al.	2022	[18]	LR, PCS
Hoad et al.	2010	[34]	PCS	Marko et al.	2022	[17]	LR, PCS
Vania et al.	2012	[13]	PS	D’Amato et al.	2022	[24]	PCS

<p><b>PS:</b> Problem Statement</p> <ul style="list-style-type: none"> <li>• flexible rotor with lubricated journal bearings;</li> <li>• fluid dynamics;</li> <li>• self-excited vibrations due to fluid dynamics;</li> </ul>	<p><b>LR:</b> Literary Review</p> <ul style="list-style-type: none"> <li>• flexible rotor bearings control;</li> <li>• active rejection of vibrational phenomena;</li> <li>• notch filtering;</li> <li>• observer-based control;</li> </ul>	<p><b>PCS:</b> Proposed Control Strategy</p> <ul style="list-style-type: none"> <li>• adaptive noise cancellation-rejection;</li> <li>• immersion and invariance;</li> <li>• method comparison;</li> <li>• numerical analysis methods;</li> </ul>
---	---	---

A mathematical proposition for the ANC-FE is formulated and a structural proof is given under assumptions on closed-loop output signals, showing that the sinusoidal disturbance rejection is exponentially performed. Numerical simulations are presented to validate the theoretical results in silico. The simulations are designed to illustrate the adaptive rejection performance in terms of time and residual vibration amplitude. Moreover, it is shown that the proposed I&I-based asymptotical frequency estimation may have a practical application since its duration is acceptable as an initialization process. This is a training/warm-up phase for the ANC controller. In addition, in order to evaluate the order of convergence of the disturbance frequency and phase estimation error point series the iterative Inexact Newton method [36] was applied.

The main novelties of this study are summarized:

- i generalization of ANC-TC control devised in [24] to the unknown/uncertain operating frequency;
- ii application of I&I robust technique for frequency estimation (FE), considering as input an analytical reconstruction of the closed-loop output noise signals;
- iii plug-in integration of the FE module with the ANC-TC control;
- iv formulation of a mathematical proposition for the novel ANC-FE control;
- v structural proof of the proposition under assumptions on closed-loop output signals.

This paper has the following outline: Section 2 introduces the closed formulation of the rotor dynamics model and ANC-FE control conceptualization and design; in Section 3 the theoretical proposition is formulated and its proof is given; Section 4 reports numerical simulation results with a detailed description of the data fitting analysis; in Section 5 the numerical simulation results are discussed and some conclusions are reported.

## 2. Materials and Methods

The dynamical system under investigation is composed by an unbalanced thin disk, symmetrically disposed on a flexible shaft, and supported by two hydrodynamic full (short) journal bearings, as represented in [24]. The mass of the rotor is 2 m and the flexible shaft is a thin bar of a circular section with a negligible mass with respect to the disk mass. According to Figure 1, during the motion, the disk remains in plane motion in x–y plane without gyroscopic effects. The lubricated dynamical system can be studied by applying the classical approach based on the Reynolds equation [20] in cylindrical coordinates and under the classical hypothesis of short bearing approximation [30]. The scalar nonlinear differential motion equations of the system are [20]

$$\begin{cases} m\ddot{x} + k(x_c - x_j) = mu\omega^2 \sin\omega t \\ m\ddot{y} + k(y_c - y_j) = -mu\omega^2 \cos\omega t - W \\ F_x(x_j, \dot{x}_j, y_j, \dot{y}_j) = -k(x_c - x_j) \\ F_y(x_j, \dot{x}_j, y_j, \dot{y}_j) = -k(y_c - y_j) \end{cases} \tag{1a}$$

where the forces  $F_x, F_y$  are defined in [24].

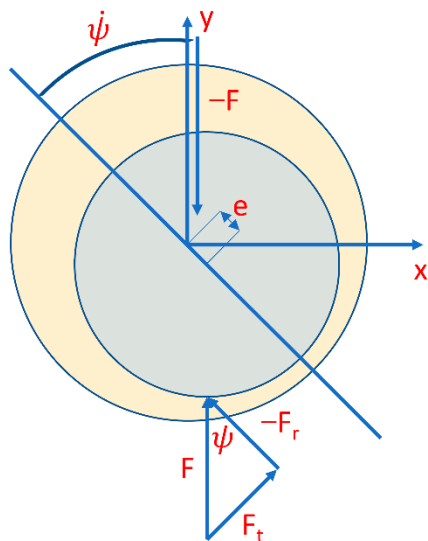


Figure 1. Journal bearing geometry.

### 2.1. Adaptive Noise Cancellation Tracking Control (ANC-TC)

In the following, for the lubricated dynamical system, the cavitating ( $\pi$ -film) and the uncavitating short bearing model are considered. A closed-form model formulation for the controlled model, which has been introduced in [24], is written as follows

$$\begin{cases} \ddot{x}(t) = \begin{bmatrix} \ddot{x}_c \\ \ddot{y}_c \end{bmatrix} \doteq -\frac{k}{m}(x - z_j) - d_w - \ddot{d}_e(t, \omega) + \vec{u}_x \\ \dot{z}_j(t, \omega, i) = \begin{bmatrix} \dot{x}_j \\ \dot{y}_j \end{bmatrix} \doteq ke^3 l^{-1}(t, z_j, e, i) \left\{ \Sigma(t, z_j, e, \omega, i) \begin{bmatrix} x_j \\ y_j \end{bmatrix} + \frac{1}{\mu_0} \begin{bmatrix} x_c \\ y_c \end{bmatrix} \right\} \end{cases} \tag{1b}$$

where:  $x = (x_c, y_c)^T$  and  $z_j = (x_j, y_j)^T$  denote the disc center and journal center coordinates, respectively;  $d_w = [0, W/m]^T$  is a constant load term and  $\vec{u}_x$  is the control input. The vector of sinusoidal disturbances acting on the two coordinate dynamics is denoted by  $d_e(t, \omega) = u[\sin(\omega t + \varphi_{01}), -\cos(\omega t + \varphi_{02})]^T$  ( $\varphi_{01,2}$  unknown initial phase), so that

$$\dot{d}_e(t, \omega) = \Omega \cdot d_e(t, \omega) \quad \Rightarrow \quad \dot{d}_e(t, \omega) = \begin{bmatrix} 0 & -\omega \\ \omega & 0 \end{bmatrix} \cdot \begin{bmatrix} u \sin(\omega t + \varphi_{01}) \\ -u \cos(\omega t + \varphi_{02}) \end{bmatrix} \tag{2}$$

The dynamics of acceleration noise in Equation (2) has the canonical parametrization ( $\Omega$ ) of a disturbance with ellipsoidal trajectories, whose dimensions depend on the values of the system parameters, as found by the numerical simulations of the analytical model Equation (1a) presented in [24,29]. The  $\omega$  is the frequency of the disturbance and corresponds to the operating rotation speed of the flexible rotor. The two matrices  $l^{-1}$  and  $\Sigma$  are defined as follows

$$l^{-1}(t, z_j, e, i) \cdot \Lambda^{-1}(t, z_j, e, i) = i \left\{ \left[ \begin{pmatrix} zx_j & -2\zeta\pi^{(i-1)}ey_j \\ zy_j & +2\zeta\pi^{(i-1)}ex_j \end{pmatrix} + (1-i) \cdot 8\lambda \begin{pmatrix} -y_j & ex_j \\ x_j & ey_j \end{pmatrix} \right] \cdot \begin{pmatrix} ex_j & ey_j \\ -y_j & x_j \end{pmatrix} \right\}^{-1} \tag{3}$$

$$\Sigma(t, z_j, e, \omega, i) \begin{pmatrix} -\frac{1}{\mu_0} & -\omega\frac{\zeta}{k}\frac{\pi}{i}^{(i-1)} \\ \omega\frac{\zeta}{k}\frac{\pi}{i}^{(i-1)} & -\frac{1}{\mu_0} \end{pmatrix} + (1-i) \cdot \begin{pmatrix} \frac{2\lambda}{k}\omega & \frac{t_0}{ke} \\ -\frac{t_0}{ke} & \frac{2\lambda}{k}\omega \end{pmatrix}$$

where:  $e = \sqrt{x_j^2 + y_j^2}$  denotes the orbit eccentricity; the  $i \in \{1, 2\}$  is the summary index, which allows us to switch the model representation among uncavitated ( $i = 1$ ) and cavitated ( $i = 2$ ) operating conditions, respectively. In [1], it was shown-analytically and by numerical simulations- that the dynamical time-variant matrix  $\Lambda$  is always nonsingular with a high determinant.

To reduce Equation (1a) into Equations (1b)–(3), the following analytical positions are introduced in [24]

$$\begin{aligned} z &= \frac{2\pi\zeta(1+2e^2)}{(1-e^2)} & \zeta &= \frac{1}{2(1-e^2)^{3/2}} & \mu_0 &= \mu R \left(\frac{l}{c}\right)^3 \\ \sigma &= \frac{e}{(c^2-e^2)^{1/2}} & \lambda &= \sigma\zeta \\ \rho_0 &= 2RLp_0 & \varepsilon &= \frac{e}{c} & t_0 &= \frac{\rho_0}{\mu_0} \end{aligned} \tag{4}$$

where:  $k, m, \mu, R, L, c, \pi, p_0, u$  are dynamical and geometrical parameters of the system collected in Table 1 [24].

In the case of known operating frequency  $\omega$ , in [24] the closed-loop ANC-TC algorithm  $\vec{u}_x$  in Equations (5)–(7) was proposed for the flexible rotor Equations (1a) and (2), and an exponential tracking of a desired trajectory for the disc center  $[\vec{x}_r; \dot{\vec{x}}_r; \ddot{\vec{x}}_r] = [x_{cr}, y_{cr}; \dot{x}_{cr}, \dot{y}_{cr}; \ddot{x}_{cr}, \ddot{y}_{cr}]$  is obtained (the detailed formal proof is reported in [24]). The ANC-TC includes two main parts: it allows both the sinusoidal disturbance in closed-loop and the springback force contribution to be adaptively canceled due to the always nonzero displacement between disc and journal (eccentricity). The overall vectorial control law is reported in Equations (5)–(7) (the vector symbols are omitted for convenience)

$$\begin{cases} u_x \triangleq \hat{u}_{x0} + \ddot{\hat{d}}_e(t, \omega) \\ \hat{u}_{x0} \triangleq \frac{k}{m}x + d_w + \hat{v}_x \\ \hat{v}_x \triangleq -\frac{k}{m}\hat{z}_j + \ddot{x}_r - k_1\dot{\tilde{x}} - k_2\tilde{x} \end{cases} \tag{5}$$

$$\begin{cases} \ddot{\hat{d}}_e(t, \omega) \triangleq \omega^2 \begin{bmatrix} -u\sin(\omega t + \hat{\phi}(t)) \\ u\cos(\omega t + \hat{\phi}(t)) \end{bmatrix} \\ \hat{\phi}(t, \omega) \triangleq \int_0^t \left( \phi(\tau, \omega) \begin{bmatrix} k_{\phi_1} & 0 \\ 0 & k_{\phi_2} \end{bmatrix} \cdot \left( \omega^2 \tilde{d}_e(\tau, \omega) \right) \right) d\tau = \left( \phi(\tau, \omega) \begin{bmatrix} k_{\phi_1} & 0 \\ 0 & k_{\phi_2} \end{bmatrix} \cdot \left( \ddot{\tilde{x}} + k_1\dot{\tilde{x}} + k_2\tilde{x} \right) \right) d\tau \\ \phi(t, \omega) \triangleq u \begin{bmatrix} \cos(\omega t + \phi_0) & 0 \\ 0 & \sin(\omega t + \phi_0) \end{bmatrix} \end{cases} \tag{6}$$

$$\begin{cases} \hat{z}_j \triangleq -\frac{m}{k}(\hat{\eta} + c_\eta \cdot \dot{x}) \\ \dot{\hat{\eta}} \triangleq -c_\eta \cdot \hat{v}_x + c_\eta \cdot \hat{\eta} + c_\eta^2 \cdot \dot{x} \end{cases} \Rightarrow \hat{\eta}(0) = 0, \quad \hat{z}_j \triangleq -\frac{m}{k} \cdot c_\eta \cdot \dot{x}(0), \tag{7}$$

where:  $\tilde{x} = (x - x_r), \dot{\tilde{x}} = \dot{x} - \dot{x}_r, \ddot{\tilde{x}} = \ddot{x} - \ddot{x}_r$  are the tracking errors of position, velocity and acceleration of disc center, respectively;  $\hat{d}_e(t, \omega)$  is the sinusoidal disturbance estimate;

$\hat{\varphi}(t) = [\hat{\varphi}_1, \hat{\varphi}_2]^T$  is the phase estimate vector, which is responsible for matching at steady-state the initial conditions of the noise ( $\overline{\varphi}_0 = [\varphi_0, \varphi_0]^T = [\varphi_{01}, \varphi_{02}]^T$ ) in (2), provided that the amplitude ( $u$ ) and frequency ( $\omega$ ) are known;  $\varphi_0 = \hat{\varphi}_i(0) = \text{rand}(-2\pi, 2\pi)$  is a random value chosen as the (arbitrary) initial value for the phase estimation. According to [24],  $\omega^2 \tilde{d}_e = \ddot{\tilde{x}} + k_1 \dot{\tilde{x}} + k_2 \tilde{x}$  is a known term, which has been modeled in Equation (6) in terms of residual spurious dynamics, under the assumption that the asymptotic control  $\hat{u}_{x0}$ —linked to the estimation of the displacement Equation (7)—is already converged on target value. Equation (6) is written according to a linear parametrization of the estimation error  $\tilde{d}_e(t, \omega) = d_e - \hat{d}_e$  [37]: it appears as product of regressor  $\Phi(t, \omega)$  and the parameter estimation error, namely  $\tilde{d}_e = \Phi^T(t, \omega) \cdot \tilde{\varphi}(t)$  (see [24]).

The control gains  $k_1, k_2, k_{\varphi_1}, k_{\varphi_2}$  and  $c_\eta$  are found by trial-and-error procedures reported in Table 2.

**Table 2.** Simulation parameters.

Dynamical Parameters	Values	Initial Conditions	Values	Operating Parameters	Values
$m$ (kg)	1.5	$x_c(0)$	0	$f$ (Hz)	500
$K$ (N/m)	$4 \times 10^6$	$\dot{x}_c(0)$	0	$\omega$ (rad/s)	3141
$u$ (m)	$10^{-3}$	$y_c(0)$	$-10^{-5}$	$\mu_0$ (m kg/s)	$7.06 \times 10^4$
$R$ (m)	$1.6 \times 10^{-2}$	$\dot{y}_c(0)$	0	$\rho_0$ (N)	$1 \times 10^{-3}$
$L$ (m)	$1.6 \times 10^{-2}$	$x_j(0)$	0	$t_0$ (s <sup>-1</sup> )	$1.45 \times 10^{-8}$
$\mu$ (kg/s)	$3.4 \times 10^{-2}$	$y_j(0)$	$-10^{-5}$	$p_0$ (bar)	2
$c$ (m)	$3.16 \times 10^{-5}$	$\varphi_0$ (rad)	[5.2, 5.2]		
$g$ (m/s <sup>2</sup> )	9.81				
$\pi$	180°				
	Step		$5 \times 10^{-6}$		
	Time (s)		12		

The phase estimator part of Equation (6) is devised since the main problem in sinusoidal noise rejection is the knowledge of the initial disturbance phase [27,38], so it acts as a dynamic Phase-Locked-Loop (PLL [39]). The displacement estimation part of Equation (7) represents a reduced-order observer of the dynamical subsystem  $[\dot{x}_c, \dot{y}_c, x_j, y_j]$  of the overall system Equation (1b). It is required due to technical limitation to install a sensor to measure the center position of the journal. For the same reasons, moreover, even if an analytical value of  $z_j$  was considered by Equation (1b), even in this case, the uncertainty on the initial condition  $z_{j0} = z_j(0)$  may have a fundamental role in the vibration attenuation at steady-state.

**Remark 1.** *It is noteworthy that only the disc center position ( $x$ ), speed ( $\dot{x}$ ) and acceleration ( $\ddot{x}$ ) measurements are required and fed back for control closed-loop adaptation Equation (7), as well as for frequency estimation (Figure 2).  $\diamond$*

**2.2. Adaptive Noise Cancellation with Frequency Estimation (ANC-FE) Control**

Now, even if the operating frequency was known, which is used as a parameter in the ANC-TC [24], it can be affected by a percentage uncertainty due to possible miscalibration of the actuator, which is keeping the rotor in rotation at  $\omega$  speed. In practice, this makes the operating frequency, and consequently the disturbance frequency, unknown. Moreover, other incoming nonlinear phenomena, such as gyroscopic moments acting on the disk, for example, due to asymmetries of the rotor support [31], can make the operating frequency vary. For this scope, consider the problem of estimating the operating frequency of the system. The following control scheme is adopted (Figure 2). The scheme recovers the one adopted in [24], where the exosystem Equation (2) (hereafter EXO) acts as an external dynamics. Downstream of the control loop, a further stage is added: the frequency



two injection terms  $[\beta_\epsilon(y), \beta_\zeta(y, \hat{\epsilon})]$  acting as a dynamical correction;  $\alpha_\epsilon = (k_\epsilon^2 + \zeta) > 0$  acts a kind of scaling. The Equation (9) is written as follows

$$\epsilon = -z_\epsilon(y) + \hat{\epsilon} (\alpha_\epsilon) + \beta_\epsilon(y); \quad \zeta = -z_\zeta(y) + \hat{\zeta} + \beta_\zeta(y, \hat{\epsilon}). \tag{10}$$

By setting at zero the estimation errors  $z_\epsilon(y), z_\zeta(y)$  in Equations (9) and (10), it follows that

$$\epsilon_{est} = (k_\epsilon^2 + \zeta_{est}) \hat{\epsilon} + k_\epsilon y; \zeta_{est} = \hat{\zeta} + y \hat{\epsilon}, \tag{11}$$

where,  $\epsilon_{est}(0) = (k_\epsilon^2 + \zeta_{est}(0)) \hat{\epsilon}(0) + k_\epsilon y(0)$  and  $\zeta_{est}(0) = \hat{\zeta}(0) + y(0) \hat{\epsilon}(0)$ .

The two asymptotic estimates  $[\epsilon_{est}, \zeta_{est}]$  are found as with a PI (proportional integral) law with respect to the measured output  $y$ . Indeed, both  $(\alpha_\epsilon) \hat{\epsilon}$  and  $\hat{\zeta}$  turn out to be an integration process,  $\alpha_\epsilon$  denotes the gain of the integral part, while both the two injection terms represent the proportional part. To prove this point, derive in time the errors  $[z_\epsilon, z_\zeta](y)$  in Equation (9). From Equation (8) it follows that

$$\dot{z}_\epsilon(y) = (\alpha_\epsilon) \dot{\hat{\epsilon}} + \zeta y + k_\epsilon \epsilon; \dot{z}_\zeta(y) = \dot{\hat{\zeta}} + \epsilon \hat{\epsilon} + y \dot{\hat{\epsilon}}, \tag{12}$$

while, replacing Equation (10) in Equation (12), it follows

$$\begin{aligned} \dot{z}_\epsilon &= (k_\epsilon^2 + \zeta) \dot{\hat{\epsilon}} + \zeta y + k_\epsilon (-z_\epsilon + k_\epsilon^2 \hat{\epsilon} + \hat{\epsilon} \zeta + k_\epsilon y) \\ &= -k_\epsilon z_\epsilon + (k_\epsilon^2 + \zeta) \left\{ y + k_\epsilon \hat{\epsilon} + \dot{\hat{\epsilon}} \right\}; \end{aligned} \tag{13a}$$

$$\begin{aligned} \dot{z}_\zeta &= \dot{\hat{\zeta}} + y \dot{\hat{\epsilon}} + \hat{\epsilon} [-z_\epsilon + k_\epsilon^2 \hat{\epsilon} + k_\epsilon y + \hat{\epsilon} (-z_\zeta + \hat{\zeta} + y \hat{\epsilon})] \\ = -\hat{\epsilon} z_\epsilon - \hat{\epsilon}^2 z_\zeta + \left\{ \dot{\hat{\zeta}} - [-y \dot{\hat{\epsilon}} - k_\epsilon^2 \hat{\epsilon}^2 - k_\epsilon y \dot{\hat{\epsilon}} - \hat{\epsilon}^2 \dot{\hat{\zeta}} - y \hat{\epsilon}^3] \right\} &= -\hat{\epsilon} z_\epsilon - \hat{\epsilon}^2 z_\zeta + \left\{ \dot{\hat{\zeta}} - \Delta(y, \hat{\epsilon}, \hat{\zeta}) \right\}. \end{aligned} \tag{13b}$$

The term  $\Delta(y, \hat{\epsilon}, \hat{\zeta})$  is a function of known signals. By setting at zero the quantities between braces in both Equations (13a) and (13b), the two scalar adaptation laws for  $(\hat{\epsilon}, \hat{\zeta})(t)$  are found as follows

$$\dot{\hat{\epsilon}} = -y - k_\epsilon \hat{\epsilon}, \quad \dot{\hat{\zeta}} = -[y \dot{\hat{\epsilon}} + k_\epsilon^2 \hat{\epsilon}^2 + k_\epsilon y \dot{\hat{\epsilon}} + \hat{\epsilon}^2 \dot{\hat{\zeta}} + y \hat{\epsilon}^3], \tag{14}$$

where, from Equations (6) and (8),  $\hat{\epsilon}(0) = u \omega_0 \cos(\omega_0 t + \hat{\varphi}_i(0))$  and  $\hat{\zeta}(0) = \omega_0^2$ .

Consequently, Equations (13a) and (13b) become

$$\begin{bmatrix} \dot{z}_\epsilon \\ \dot{z}_\zeta \end{bmatrix} = \begin{bmatrix} -k_\epsilon & 0 \\ -\hat{\epsilon} & -\hat{\epsilon}^2 \end{bmatrix} \cdot \begin{bmatrix} z_\epsilon \\ z_\zeta \end{bmatrix}. \tag{15}$$

The first-row of Equation (15) makes that  $z_\epsilon \rightarrow 0$  exponentially. However, this is not sufficient to construct an estimation of the state variable  $\epsilon$  since the overall convergence of the estimation is linked to the convergence of all the error dynamics  $[z_\epsilon, z_\zeta]$ . However, once the two adaptation laws have reached their steady-state values, namely  $[\dot{\hat{\epsilon}}, \dot{\hat{\zeta}}] = [0, 0]$ , the asymptotic estimates for  $[\epsilon_{est}, \zeta_{est}] = [\epsilon, \omega^2]$  are given by Equation (11) (see the proof in Section 3). Note that  $\omega_0$  may be the rough initial estimate of the operating rotor frequency, taken from the rotor actuator datasheet as the steady-state operation value. As mentioned above, the estimates of Equation (11) are two PI, with integral parts  $(\alpha_\epsilon) \hat{\epsilon}$  and  $\hat{\zeta}$ , as may be inferred from Equation (14).

### 2.2.2. ANC-FE Control Design with Analytical Output Noise ( $y_{an}$ )

Regarding the assumption about  $y$ , which in Equations (8)–(14) is regarded as the measured output of the closed-loop system Equations (1a)–(7), it requires a sensor in output able to distinguish and provide only the sinusoidal vibration measurement ( $d_e(t, \omega)$ ). First, it is a logic short-circuit since once the disturbance measurement is available a direct cancellation could be viable. Second, the sensor in turn may be affected by measurement

noise, which is source of uncertainty. Then, the ANC-FE control Equations (8)–(14) with measured output noise  $(y(t, \omega))$  cannot be directly implemented in closed-loop. For this scope, the value of the output noise  $y$ , which is used as a known quantity in the ANC-FE Equations (8)–(14), is reconstructed analytically from Equation (1b). By using position, speed and acceleration measurements of the disc center coordinates  $([\ddot{x}, \dot{x}, x]^T)$  and an analytical chasing of the journal center displacement  $(\bar{z}_j(\omega_0))$ , the analytical output noise  $(y_{an})$  is computed from Equations (1b)–(3) as follows

$$y_{an}(t, \bar{z}_j, \hat{\omega}) = \left\{ \ddot{x}(t) + \frac{k}{m}(x - \bar{z}_j(t, \hat{\omega}(t))) + d_w - \vec{u}_x \right\} \tag{16}$$

$$\bar{z}_j(t, \hat{\omega}(t), i) \bar{z}_{j0} + \int_0^t \left[ k \bar{e}^3 l^{-1}(\tau, \bar{z}_j, \bar{e}, i) \left\{ \Sigma(\tau, \bar{z}_j, \bar{e}, \hat{\omega}(\tau), i) \bar{z}_j(\tau, \hat{\omega}(\tau)) + \frac{1}{\mu_0} x(\tau) \right\} \right] d\tau \tag{17}$$

where:  $\bar{z}_{j0}$  is the arbitrary initial condition of the analytical chasing  $\bar{z}_j(t, \hat{\omega}(t), i)$  of the journal displacement  $(z_j)$ ;  $z_j(t, \omega, i)$  is a function of the frequency through the matrix  $\Sigma(t, z_j, e, \omega, i)$  in Equation (3);  $\bar{e}$  is the eccentricity computed in the analytical chasing coordinates  $(\bar{z}_j)$ . From Equations (1b) and (16), it follows

$$y_{an}(t, \bar{z}_j, \hat{\omega}) = \begin{bmatrix} \vdots \\ y_{ani} \\ \vdots \end{bmatrix} \doteq \ddot{d}_e(t, \omega) + \frac{k}{m} [-z_j(t, \omega) + \bar{z}_j(t, \hat{\omega}(t))] = \ddot{d}_e(t, \omega) + \delta_y(t, \bar{z}_{j0}, \omega, \hat{\omega}(t)) \equiv y_{an}(t, \bar{z}_j, \omega, \hat{\omega}) \tag{18}$$

where from (8)  $\ddot{d}_{ei}(\omega, t) \propto d_{ei} = y$ , so that  $y_{ani} \propto \ddot{d}_{ei}(\omega, t)$ . The constant proportional factor is the square of unknown frequency  $-\omega^2$ , which, from (11), is absorbed in the tuning procedure of  $k_e$ . Then,  $y_{an}$  and the bounded disturbance  $d_e(t, \omega)$  are consistent since, eventually, the two sinusoidal vibrations have the same frequency  $(\omega)$ . Indeed, from Equation (18),  $y_{an}(t, \bar{z}_j, \omega, \hat{\omega})$  is a function of  $\omega$ . We now state the main assumption in this paper.

**Assumption 1.** *The analytical chasing error  $\delta_y(t, \bar{z}_{j0}, \omega, \hat{\omega}(t))$  in Equation (18) is bounded and small enough that  $y_{an}(t, \bar{z}_j, \hat{\omega})$  is assumed at the same frequency of  $\dot{d}_e(t, \omega) = \Omega d_e(t, \omega)$ . ▼*

From Equations (8) and (16)–(18), according to Remark 2, and under the Assumption 1, the asymptotic adaptation laws Equations (11)–(14) are updated considering the computation for only one component  $y_{ani}$ , as follows

$$\begin{aligned} \epsilon_{est} &= (k_e^2 + \zeta_{est}) \hat{\epsilon} + k_e y_{ani} i \\ \zeta_{est} &= \hat{\zeta} + y_{ani} \hat{\epsilon}; \dot{\hat{\epsilon}} = -y_{ani} - k_e \hat{\epsilon}; \dot{\hat{\zeta}} = - \left[ y_{ani} \hat{\epsilon} + k_e^2 \hat{\epsilon}^2 + k_e y_{ani} \hat{\epsilon} + \hat{\epsilon}^2 \hat{\zeta} + y_{ani} \hat{\epsilon}^3 \right], \end{aligned} \tag{19}$$

$$\text{with } \omega_{est} = \lim_{t \rightarrow \infty} \hat{\omega}(t) = \lim_{t \rightarrow \infty} \sqrt{\zeta_{est}(t)}$$

$$\text{with } \epsilon_{est}(0) = (k_e^2 + \zeta_{est}(0)) \hat{\epsilon}(0) + k_e y_{ani}(0); \zeta_{est}(0) = \hat{\zeta}(0) + y_{ani}(0) \hat{\epsilon}(0);$$

$$\hat{\epsilon}(0) = u \omega_0 \cos(\omega_0 t + \hat{\phi}_i(0)); \hat{\zeta}(0) = \omega_0^2.$$

Equations (16), (17), and (19), constitute the frequency estimator (FE) equations. Equation (15) holds as function of  $y_{ani}$ .

By absorbing Equations (16), (17) and (19) in the ANC-TC Equations (5)–(7), the ANC-FE control, Equations (19)–(20c) with analytical output noise  $(y_{an}(t, \bar{z}_j, \hat{\omega}))$ , is implementable in closed-loop as follows

$$\begin{cases} \hat{u}_x \triangleq \hat{u}_{x0} + \ddot{d}_e(t, \omega_{est}) \\ \hat{u}_{x0} \triangleq \frac{k}{m} x + d_w + \hat{\vartheta}_x \\ \hat{\vartheta}_x \triangleq -\frac{k}{m} \hat{z}_j + \ddot{x}_r - k_1 \dot{\hat{x}} - k_2 \hat{x} \end{cases} \tag{20a}$$

$$\left\{ \begin{aligned} \ddot{\hat{d}}_e(t, \omega_{est}) &\triangleq \omega_{est}^2 \begin{bmatrix} -u & \sin(\omega_{est}t + \hat{\phi}(t)) \\ u & \cos(\omega_{est}t + \hat{\phi}(t)) \end{bmatrix} \\ \hat{\phi}(t, \omega_{est}) &\triangleq \int_0^t \left( \varphi(\tau, \omega_{est}) \begin{bmatrix} k_{\varphi 1} & 0 \\ 0 & k_{\varphi 2} \end{bmatrix} \cdot \left( \ddot{\tilde{x}} + k_1 \dot{\tilde{x}} + k_2 \tilde{x} \right) \right) d\tau \\ \varphi(t, \omega_{est}) &\triangleq u \begin{bmatrix} \cos(\omega_{est}t + \phi_0) & 0 \\ 0 & \sin(\omega_{est}t + \phi_0) \end{bmatrix} \end{aligned} \right. \quad (20b)$$

$$\left\{ \begin{aligned} \hat{z}_j &\triangleq -\frac{m}{k} (\hat{\eta} + c_\eta \cdot \dot{x}) \\ \dot{\hat{\eta}} &\triangleq -c_\eta \cdot \hat{v}_x + c_\eta \cdot \hat{\eta} + c_\eta^2 \cdot \dot{x} \end{aligned} \right. \Rightarrow \hat{\eta}(0) \doteq 0, \quad \hat{z}_j \triangleq -\frac{m}{k} \cdot c_\eta \cdot \dot{x}(0), \quad (20c)$$

where, in Equations (20a)–(20c), the asymptotic estimate  $\omega_{est} = \hat{\omega}(t)_{t \rightarrow \infty}$  (Equation (19)) is considered for the constant  $\omega$  as the constant frequency parameter in the phase estimator (compare Equations (5)–(7) with Equations (20a)–(20c)).

At steady-state, when all the estimates’ terms are converged (i.e.,  $\hat{v}_x \rightarrow v_x, \hat{z}_j \rightarrow z_j, \hat{d}_e \rightarrow d_e$ ), the closed-loop system, Equations (1b)–(4) and (19)–(20c), is regulated by  $\hat{u}_x \rightarrow u_x$  around the reference  $x_r$  (Figure 2).

**Remark 3.** The idea of frequency estimation, namely Equations (8)–(15), inspired from immersion and invariance (I&I) approach, are borrowed from the algorithm proposed in [32]. Nevertheless, the novelty of applying this technique to a rotordynamic model Equation (1a) [24,30] consists of a further manipulation. Equations (16)–(19) have been introduced with the aim of reconstructing analytically ( $y_{an}$ ) an unavailable signal, the output noise ( $y$ ). The signal chasing Equation (17) is possible by virtue of the closed-form formulation, Equations (1b)–(4), presented in [24], which allows a reliable numerical extraction of the coordinates of the journal disc center to be performed, with a very high determinant value of the matrix  $\Lambda$ , by integration of Equation (1b).

In particular, the system Equation (8) of dimension 3 [ $\zeta, \epsilon, y_{ani}$ ] is immersed in a wider space with 5 dimensions [ $\zeta, \xi, \epsilon, \hat{\epsilon}, y_{ani}$ ]. Then, the observer problem is attracted by the surface at  $z_\epsilon = 0$  and  $z_\zeta = 0$ , where it remains at steady-state, so that the resultant invariant locus is a manifold (Figure 3).  $\diamond$

**Remark 4.** It is worth highlighting that Equation (20c) is identical to Equation (7), namely, the reduced-order-observer, which estimates the  $z_j$  displacement, acts independently from the other control blocks. The FE controller designed in this paper (Equations (16)–(19)) based on the analytical output  $y_{an}$  results as a plug-in estimation block downstream to the ANC-TC Equations (5)–(7) proposed in [24]. This property shall be exploited for control convergence proof.  $\diamond$

**Remark 5.** The control ANC-FE Equations (19) and (20a)–(20c) are a general-purpose control with respect to the actual lubricated rotordynamics’ operating condition, namely cavitated/uncavitated. Indeed, according to the notations in Equations (1b)–(4), the matrices  $l^{-1}(t, \bar{z}_j, \bar{v}, i)$  and  $\Sigma(t, \bar{z}_j, \bar{v}, \hat{\omega}(t), i)$  in Equation (17) are functions of the parameter  $i$ .  $\diamond$

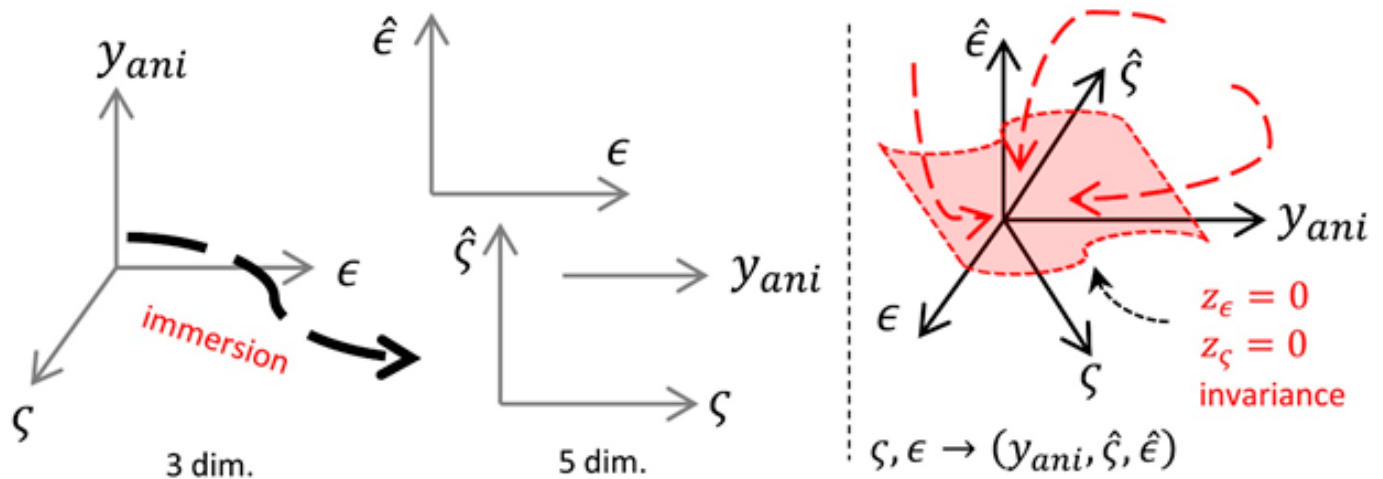


Figure 3. Immersion and Invariance application on analytical output noise ( $y_{ani}$ ).

### 3. Closed-Loop ANC-FE Control Convergence Proof

#### 3.1. Proposition Statement

In this section a formal convergence proof of the proposed closed-loop ANC-FE control Equations (19) and (20a)–(20c) is provided through the following proposition statement.

**Proposition 1.** Consider the lubricated rotordynamic model Equations (1b)–(4) and  $y = d_{ei}(t, \omega)$  Equation (8) as the sinusoidal output noise from the exosystem (2), with unknown constant frequency ( $\omega$ ) and initial phase ( $\varphi_0$ ). Consider the reference dynamics  $\vec{x}_r = [x_{cr}, y_{cr}]$  for the disc center coordinates, with  $\tilde{x} = (x - x_r)$ .

From Equations (9) and (16)–(20c),  $\tilde{\varphi} = (\overline{\varphi_0} - \hat{\varphi}(t))$ ,  $\tilde{z}_j = (z_j - \hat{z}_j)$ ,  $z_\epsilon(t, y_{ani}) = (-\epsilon_{est} + (k_\epsilon^2 + \zeta_{est})\hat{\epsilon} + k_\epsilon y_{ani})$  and  $z_\zeta(t, y_{ani}) = (-\hat{\omega}^2(t) + \hat{\zeta} + y_{ani} \hat{\epsilon})$ .

Under the Assumption 1, the  $\hat{u}_x$  control in Equations (20a)–(20c) makes that for the closed-loop system Equations (1b)–(4) and (19)–(20c):

- i. the equilibrium point  $(z_\epsilon(y_{ani}), \hat{\epsilon}(y_{ani})z_\zeta(y_{ani})) = (0, 0)$  is asymptotically stable;
- ii.  $\epsilon_{est} = (k_\epsilon^2 + \zeta_{est})\hat{\epsilon} + k_\epsilon y_{ani}$  is an asymptotic estimate of the analytical output noise derivative  $\dot{y}_{ani}$  and  $\omega_{est} = \lim_{t \rightarrow \infty} \hat{\omega}(t) = \sqrt{\hat{\zeta} + y_{ani} \hat{\epsilon}}$  is an asymptotic estimate of the rotor operating frequency  $\omega$ ;  $\square\square$
- iii.  $(\tilde{\varphi}, \tilde{z}_j, \tilde{x}) = (0, 0, 0)$  is exponentially stable (thesis from [24]).  $\square\square\square$

#### 3.2. Proof

Let  $V_1(t, z_\epsilon, z_\zeta)$  be a suitable Lyapunov function

$$V_1(t, z_\epsilon, z_\zeta) = \frac{z_\epsilon^2}{2k_\epsilon} + \frac{z_\zeta^2}{2} \geq 0. \tag{21}$$

Deriving in time Equation (21), from Equation (15)

$$\dot{V}_1(t, z_\epsilon, z_\zeta) = -z_\epsilon^2 - \hat{\epsilon}z_\zeta z_\epsilon - \hat{\epsilon}^2 z_\zeta^2 = - \begin{bmatrix} z_\epsilon & \hat{\epsilon}z_\zeta \end{bmatrix} \begin{bmatrix} 1 & \frac{1}{2} \\ \frac{1}{2} & 1 \end{bmatrix} \begin{bmatrix} z_\epsilon \\ \hat{\epsilon}z_\zeta \end{bmatrix} \leq 0, \quad \forall (z_\epsilon, \hat{\epsilon}z_\zeta). \tag{22}$$

Due to  $\dot{V}_1 \leq 0$ ,  $V_1(t, z_\epsilon, z_\zeta)$  is always nonincreasing in  $t \in (0, \infty)$ , so that  $V_1$  is bounded and, consequently,  $(z_\epsilon, z_\zeta)$  are bounded. By deriving in time  $\dot{V}_1$  Equation (22) and from Equations (15) and (19), it follows

$$\begin{aligned} \ddot{V}_1(t, z_\epsilon, z_\zeta) &= -2z_\epsilon \dot{z}_\epsilon - \dot{\hat{\epsilon}}z_\zeta z_\epsilon - \hat{\epsilon}\dot{z}_\zeta z_\epsilon - \hat{\epsilon}z_\zeta \dot{z}_\epsilon - (\dot{\hat{\epsilon}}^2)z_\zeta^2 - \hat{\epsilon}^2(\dot{z}_\zeta^2) \\ &= 2k_\epsilon z_\epsilon^2 - z_\zeta z_\epsilon (-y_{ani} - k_\epsilon \hat{\epsilon}) - \hat{\epsilon}z_\epsilon (-\dot{\hat{\epsilon}}z_\epsilon - \hat{\epsilon}^2 z_\zeta) + k_\epsilon \hat{\epsilon}z_\zeta z_\epsilon \\ &\quad - 2\hat{\epsilon}z_\zeta^2 (-y_{ani} - k_\epsilon \hat{\epsilon}) - 2\hat{\epsilon}^2 z_\zeta (-\dot{\hat{\epsilon}}z_\epsilon - \hat{\epsilon}^2 z_\zeta). \end{aligned} \tag{23}$$

The  $\ddot{V}_1$  is bounded since under the Assumption 1 the analytical output noise  $y_{ani}$  is bounded and the estimate  $\hat{e}(s) = [-y_{ani}(s)/(s + k_e)]$  is a passive filter of a bounded signal, so it is bounded and also its derivative  $\dot{\hat{e}} = (-y_{ani} - k_e \hat{e})$  is bounded in turn. Then, B.2.1 Barbalat’s Lemma [40] applies on  $\dot{V}_1$ , so that  $\lim_{t \rightarrow \infty} \dot{V}_1(t) = 0$ . Consequently,  $(z_e, \hat{e}z_c) \rightarrow (0, 0)$  globally asymptotically. Now, according to [32] and from Equations (10), (13) and (19),  $\epsilon_{est} = (k_e^2 + \zeta_{est})\hat{e} + k_e y_{ani}$  is an asymptotic estimate of analytical output noise derivative  $\dot{y}_{ani}$ , while  $\omega_{est} = \hat{\omega}(t)_{t \rightarrow \infty} = \sqrt{\hat{\zeta} + y_{ani}} \hat{e}$  is an asymptotic estimate of the rotor operating frequency  $\omega$ . This proves the theses (i)–(ii).

The rest of the proof is inherited from [24].

Let  $V_2(t, \tilde{\varphi})$  and  $V_3(t, \tilde{\eta})$  be introduced as two suitable Lyapunov functions

$$V_2(t, \tilde{\varphi}) = \frac{1}{2} \tilde{\varphi}^T \cdot \tilde{\varphi} \geq 0, \tag{24}$$

$$V_3(t, \tilde{\eta}) = \frac{1}{2} \tilde{\eta}^T \cdot \tilde{\eta} \geq 0. \tag{25}$$

Deriving  $V_2(t)$  Equation (24) in time, from Equations (6) and (20b) it follows

$$\dot{V}_2(t) = \tilde{\varphi}^T \dot{\tilde{\varphi}} = -\tilde{\varphi}^T \Phi(t, \omega_{est}) \begin{bmatrix} k_{\varphi 1} & 0 \\ 0 & k_{\varphi 2} \end{bmatrix} (\omega^2 \tilde{d}_e(t, \omega_{est})) = -\tilde{d}_e^T \left[ (\omega^2 k_{\varphi}) I_{(2 \times 2)} \right] \tilde{d}_e \leq 0, \tag{26}$$

where:  $k_{\varphi 1} = k_{\varphi 2} = k_{\varphi} > 0$ ;  $I_{(2 \times 2)}$  is the 2-by-2 identity matrix; the linear parametrization of the estimation error in Equation (6) has been considered, i.e.,  $\tilde{d}_e(t, \omega_{est}) = \Phi^T(t, \omega_{est}) \tilde{\varphi}(t, \omega_{est})$  (where the  $\omega_{est}$  has been considered constant at steady-state so that it is replaced for the actual constant  $\omega$ ). Due to  $\dot{V}_2 \leq 0$ ,  $V_2(t)$  does not increase in  $t \in (0, \infty)$ . Then,  $V_2$  is bounded and so  $\tilde{\varphi}$  is bounded. By time-deriving  $V_2$  again, under the assumption of bounded  $(\Phi, \dot{\Phi})$ , the Barbalat’s Lemma in [40] applies on  $\dot{V}_2$ . Then,  $\lim_{t \rightarrow \infty} \dot{V}_2(t) = 0$  and  $\tilde{d}_e \rightarrow 0$ ; consequently,  $\tilde{\varphi} \rightarrow 0$  asymptotically. To prove the exponential convergence of  $\tilde{\varphi}(t, \omega_{est})$  estimation error the Persistency of Excitation condition [40] is required, provided that  $\exists T, k_T \in \mathbb{R}^+$  such that

$$\int_t^{t+T} \Phi(\tau, \omega_{est}) \Phi^T(\tau, \omega_{est}) d\tau \geq k_T I_{(2 \times 2)} > 0, \forall t \geq 0, \tag{27}$$

which is always trivially fulfilled, given the regressor definition in Equations (6) and (20b).

Now, consider, from Equations (7) and (20c), the following definitions of  $\tilde{\eta}, \tilde{\eta}, \tilde{v}_x, \tilde{u}_x$

$$\begin{aligned} -\frac{k}{m}(z_j - \hat{z}_j) &= (c_{\eta} \dot{x} + \eta) - (c_{\eta} \dot{x} + \hat{\eta}) \tilde{\eta} \\ \dot{\eta} - \dot{\hat{\eta}} &= (-c v_x + c \eta) - (-c \hat{v}_x + c \hat{\eta}) = -c \tilde{v}_x + c \tilde{\eta} \dot{\eta}, \\ v_x - \hat{v}_x &= (u_x - \hat{u}_x) + \omega^2 \tilde{d}_e = \tilde{u}_x + \omega^2 \tilde{d}_e \tilde{v}_x \\ &\quad - \frac{k}{m} \tilde{z}_j - \omega^2 \tilde{d}_e \tilde{u}_x \end{aligned} \tag{28}$$

with  $c_{\eta} < 0$  (see [24] for detailed derivation of Equation (28)). Deriving  $V_3(t)$  Equation (25) in time, from (28) it follows

$$\begin{aligned} \dot{V}_3(t) &= \tilde{\eta}^T \cdot \dot{\tilde{\eta}} = c \cdot \tilde{\eta}^T \tilde{\eta} + (-c) \cdot \tilde{\eta}^T (\tilde{u}_x + \omega^2 \tilde{d}_e) \leq \frac{c}{2} \cdot \|\tilde{\eta}\|^2 + \left(-\frac{c}{2}\right) \left(\|\tilde{u}_x\| + \|\omega^2 \tilde{d}_e\|\right)^2 \\ &= \frac{c}{2} \cdot \|\tilde{\eta}\|^2 + \left(-\frac{c}{2}\right) \|\omega^2 \tilde{d}_e\|^2 + \left(-\frac{c}{2}\right) \left\| -\frac{k}{m} \tilde{z}_j - \omega^2 \tilde{d}_e \right\|^2 + (-c) \left\| -\frac{k}{m} \tilde{z}_j - \omega^2 \tilde{d}_e \right\| \|\omega^2 \tilde{d}_e\| \\ &\leq \frac{c}{2} \cdot \|\tilde{\eta}\|^2 + \left(-\frac{c}{2}\right) \|\omega^2 \tilde{d}_e\|^2 \left(-\frac{c}{2}\right) \left(\left\| -\frac{k}{m} \tilde{z}_j \right\| + \|\omega^2 \tilde{d}_e\|\right) \left(\left\| -\frac{k}{m} \tilde{z}_j \right\| + \|\omega^2 \tilde{d}_e\| + 2\|\omega^2 \tilde{d}_e\|\right) \\ &= -2c \|\omega^2 \tilde{d}_e\|^2 - 2c \|\tilde{\eta}\| \|\omega^2 \tilde{d}_e\| \leq c \|\tilde{\eta}\|^2 - c \omega^4 \|\tilde{d}_e\|^2. \end{aligned} \tag{29}$$

Equation (29) is obtained considering the triangular inequalities  $\tilde{\eta}^T (\tilde{u}_x + \omega^2 \tilde{d}_e) \leq \frac{1}{2} (\|\tilde{\eta}\|^2 + \|\tilde{u}_x + \omega^2 \tilde{d}_e\|^2)$  and  $\left\| \left(-\frac{k}{m} \tilde{z}_j\right) + (-\omega^2 \tilde{d}_e) \right\|^2 \leq \left(\left\| -\frac{k}{m} \tilde{z}_j \right\| + \left\| -\omega^2 \tilde{d}_e \right\|\right)^2$ ; then,

the square of  $\xi(t) \triangleq (\|\tilde{\eta}\| + \|\omega^2 \tilde{d}_e\|)$  has been reconstructed, so that the inequalities  $\|\tilde{\eta}\| \|\omega^2 \tilde{d}_e\| \leq -\frac{1}{2} (\|\tilde{\eta}\|^2 + \|\omega^2 \tilde{d}_e\|^2)$  have been used.

Following this,  $\tilde{d}_e(t)$  is bounded on  $[0, \infty)$  so that, according to Lemma A.1 in [41], any globally exponentially convergent observer for the modal disturbance  $\tilde{d}_e(t)$  guarantees the exponential convergence for  $\tilde{\eta} \rightarrow 0$  and, consequently, for  $\tilde{z}_j \rightarrow 0$  and  $\tilde{u}_x = (u_x - \hat{u}_x) \rightarrow 0$  (see Equation (28)). This is enforced by the global exponential zero convergence of  $\tilde{d}_e(t)$ , as has been proved in Equations (26) and (27).

Eventually, by replacing in Equation (1a) the control  $\hat{u}_x$  Equation (20a) ( $\hat{u}_x$  for  $u_x$ ), it follows that for  $\tilde{u}_x \rightarrow 0$

$$\ddot{\tilde{x}} = -k_1 \dot{\tilde{x}} - k_2 \tilde{x} + \frac{k}{m} \tilde{z}_j - \ddot{d}_e = -k_1 \dot{\tilde{x}} - k_2 \tilde{x} - \tilde{u}_x = -k_1 \dot{\tilde{x}} - k_2 \tilde{x} \tag{30}$$

is a Hurwitz system dynamics. Hence, also  $\tilde{x} \rightarrow 0$  globally exponentially. This proves the thesis (iii). ■■■

**Remark 6.** It has been proved that, under the Assumption 1, the convergence of asymptotical frequency estimate FE in Equation (19)—with its additional inner loop  $(\hat{\omega}(t), y_{an}(t, \bar{z}_j, \omega, \hat{\omega}))$  in which the FE is elaborated—is standalone with respect to the rest of the control loop: it is a plug-in estimation block, according to Remark 2. In this case, once  $\omega_{est} \rightarrow \omega$ , at steady-state  $\omega_{est}$  is considered as an internal parameter for the control loop. Then, the frequency estimation phase is a warm-up process for the ANC-TC Equations (5)–(7) [34,35], which through Equation (19) is transformed into Equations (20a)–(20c). ◇

**Remark 7.** From [24,32], as aforementioned at the beginning of Section 2.2.1, the closed-loop system from the input disturbance  $d_e(t)$  to the output  $x(t)$ , including the phase estimator Equation (20b), the journal displacement observer Equation (20c) and the asymptotic frequency estimator Equation (19), results in a regulation loop unifying the parameter and state estimation problems as reduced-order observed-based problems, with adaptive notch filtering characteristics [24]. ◇

## 4. Results

### 4.1. Numerical Simulation Setup and Method Description

The proposed control is implemented in the Simulink MATLAB environment with the parameter set as shown in Table 2 and with the control parameters reported in Table 3. The results are presented in four simulation cases for cavitated and uncavitated operating conditions with measured and analytical output noise.

The subscript “i” in the notation of the analytical output noise  $y_{ani}$  is omitted for editing convenience of the graphs. Hence,  $y_{an}$  in all figures is referred to as the only one component  $y_{ani}$ , accordingly to Equation (16) and Remark 2.

The signal  $\ddot{d}_{ei}(t, \omega)$  and  $z_j$  in the figures represent the actual sinusoidal disturbance and the journal center vector coordinates, respectively, whose values are computed from the simulated model differential equations. These signals,  $(\ddot{d}_{ei}(t, \omega), z_j)$  would not be available in practice, so their analytical chasing in simulation is reported only for the sake of comparison with respect to the analytical signals.

**Table 3.** Control Parameters.

Control Gains	Values	Initial Conditions	Values
$c_\eta$ [s <sup>-1</sup> ]	−400	$\hat{x}_j(0)$	0
$k_1, k_2$	2000	$\hat{y}_j(0)$	0
$k_{\varphi_1}$	50.66	$\hat{\varphi}(0)$ (rad)	[4, 4]
$k_{\varphi_2}$	50.66	$\omega_0$ (rad/s)	2985
$k_\epsilon$	7.5	$\bar{z}_{j0}$ (m)	$[0, -2 \times 10^{-5}]$

Bias and initialization issues can mislead the estimated response measure of performance obtained from a simulation. Several techniques surveyed in [34] can be used to estimate online the length of the warm-up phase in the output data collection of a simulation model, to understand, automatically, when this preliminary phase ends and when the actual numerical simulation starts giving a reliable response. The same issue is tackled in Bayesian parameter estimation [35] where the parameters of the model under study are usually derived from the available data, using optimization and sampling method estimations. It is shown that a warm-up phase occurs (the asymptotical frequency estimation phase) before the closed-loop ANC control can start its exponential hooking of the exosystem output disturbance signal. In practice, such a length cannot be quantified, but for the proposed technique, the warm-up phase length estimation is not required.

The simulations are designed in order to validate numerically the theoretical analytical proof reported in the previous Section 3. In practice, the settling time and trajectory behavior of the phase estimate can be forecast since its trend is exponential, properly, while this does not occur for the frequency estimate, which converges asymptotically. Hence, to highlight the differences in the convergence behaviors of the estimation errors, a further numerical evidence is provided. The Inexact Newton method [36] is applied to the frequency estimation error and phase estimation error successions, while the convergence of the overall disturbance error succession is considered only in the time since it follows from the previous two errors. The iterative Newton method is applied to the error successions in both cavitated and uncavitated conditions, and only in the case of analytical output noise, which is more interesting in practice.

To analyze and evaluate the order of the convergence of the estimation errors, the following point series are defined as the difference between the estimation dynamics terms and the constant target values of each series ( $\omega$  and  $\varphi_0$ ). Denoting the successions of frequency and phase estimation with  $\{\omega_{est,yan_n}\}_n$  and  $\{\hat{\varphi}_{-,yan_n}\}_n$ , respectively, sampled at discrete time instants  $n$  (1 sample each 5 (ms)), the following

$$e_{\omega_n} = \{\omega_{est,yan_n}\}_n - \omega \quad e_{\varphi_n} = \{\hat{\varphi}_{-,yan_n}\}_n - \varphi_0 \tag{31}$$

represent the successions of the frequency and phase estimation errors, respectively. Considering the absolute value of the ratio between the  $\{n + 1\}$ -element of each error succession and the  $\{n\}$ -element power of  $p_{\omega,\varphi}$ , as long as the limits of these ratios are constant for  $n \rightarrow \infty$ , namely

$$\lim_{n \rightarrow \infty} \frac{|\omega_{est,yan_{n+1}} - \omega|}{|\omega_{est,yan_n} - \omega|^{p_\omega}} = constant \quad \lim_{n \rightarrow \infty} \frac{|\hat{\varphi}_{-,yan_{n+1}} - \varphi_0|}{|\hat{\varphi}_{-,yan_n} - \varphi_0|^{p_\varphi}} = constant \tag{32}$$

then, each succession converges with at least a polynomial behavior.

We can rewrite Equation (32) as follows

$$|\omega_{est,yan_{n+1}} - \omega| \leq k_\omega \cdot |\omega_{est,yan_n} - \omega|^{p_\omega} \quad |\hat{\varphi}_{-,yan_{n+1}} - \varphi_0| \leq k_\varphi \cdot |\hat{\varphi}_{-,yan_n} - \varphi_0|^{p_\varphi} \tag{33}$$

parametrized by the coefficient pair  $(k_{\omega,\varphi}, p_{\omega,\varphi})$ . In Equation (33):  $p_{\omega,\varphi}$  represents the order of convergence for each error succession, Equations (31) and (32), while  $k_{\omega,\varphi}$  is a proportional factor, denoting the exponential convergence time-constant (when  $p_{\omega,\varphi} = 1$ ).

The following numerical simulations are proposed to: (1a) evaluate the convergence performance of disturbance estimation errors in time; (2) verify that the initial frequency estimation warm-up phase length is acceptable in practice in a real application (namely the asymptotical convergence occurs at  $t < \infty$ ). In all four simulation scenarios, 5% of initial frequency estimation error and about 25% (about 70 deg) of initial phase estimation error are considered.

4.2. Figure Descriptions

Figures 4 and 5 illustrate the frequency estimation performance in time, in the case of the cavitated condition (Figure 4) and in the case of the uncavitated condition (Figure 5). Three curves are plotted:  $\omega$  denotes the real constant operating frequency;  $\omega_{est,yan}$  denotes the asymptotical frequency estimate with the analytical output noise;  $\omega_{est,y}$  denotes the asymptotical frequency estimate in the case of measured output noise.

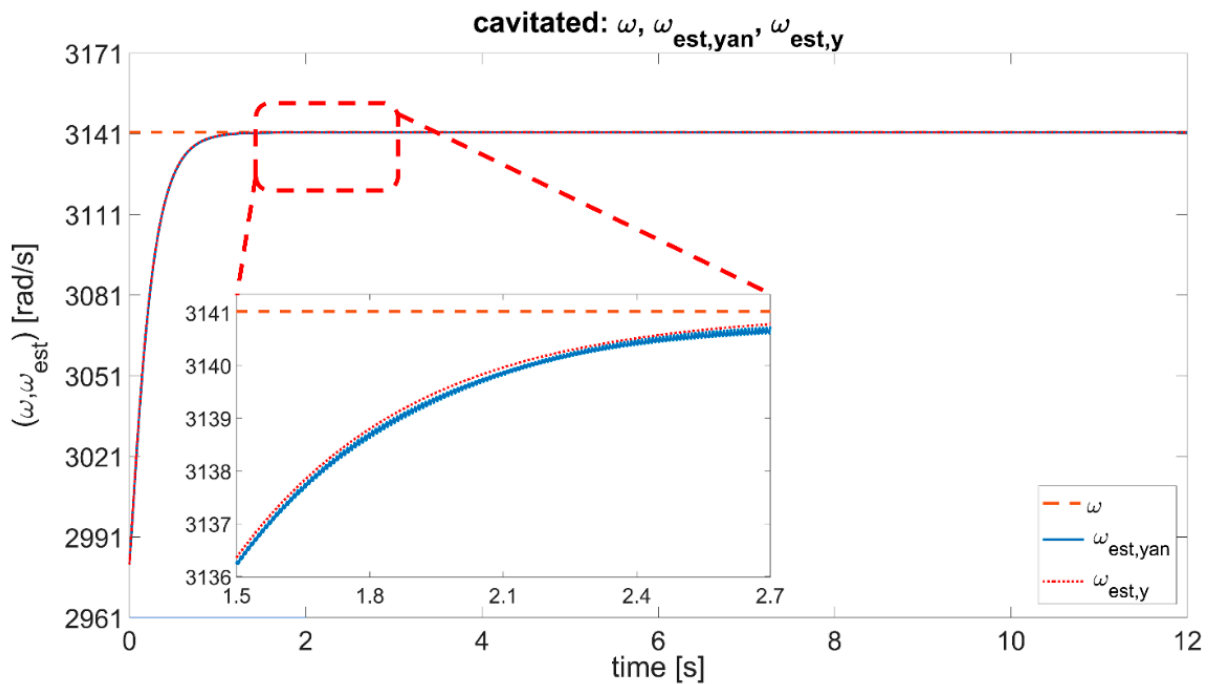


Figure 4. Frequency estimation performance in the case of cavitated condition.

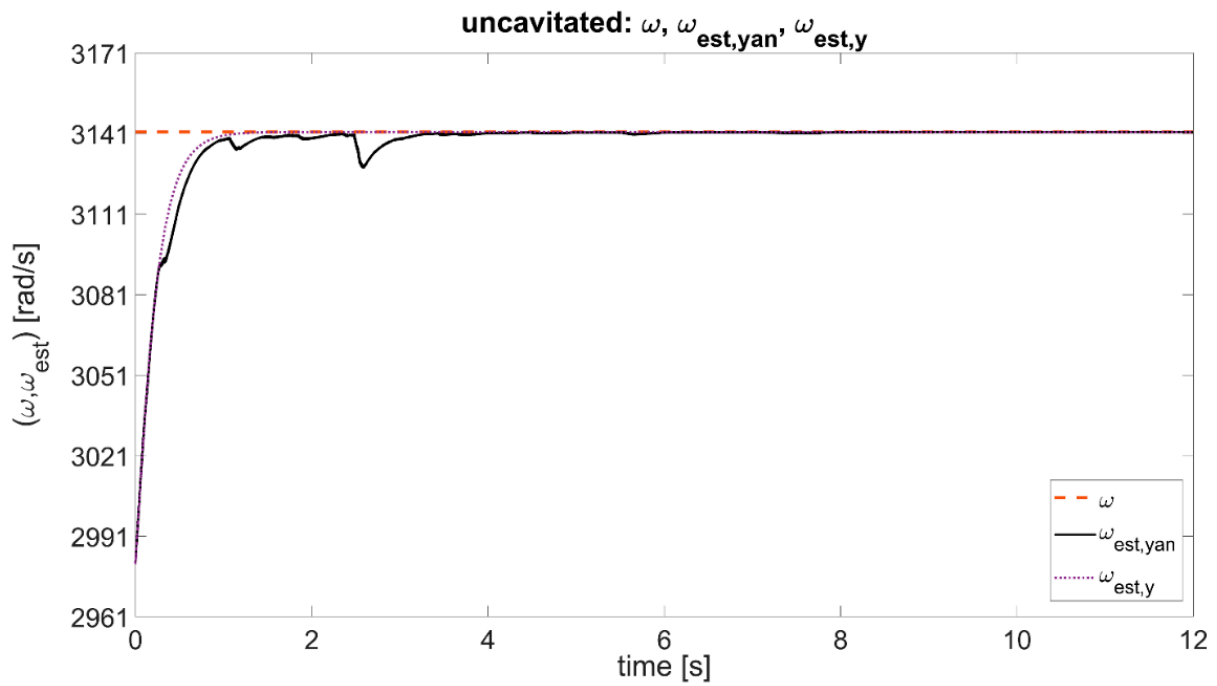


Figure 5. Frequency estimation performance in the case of uncavitated condition.

In Figure 6 the frequency estimation performance in time, considering the analytical output noise  $y_{an}$ , is compared in uncavitated and cavitated conditions.

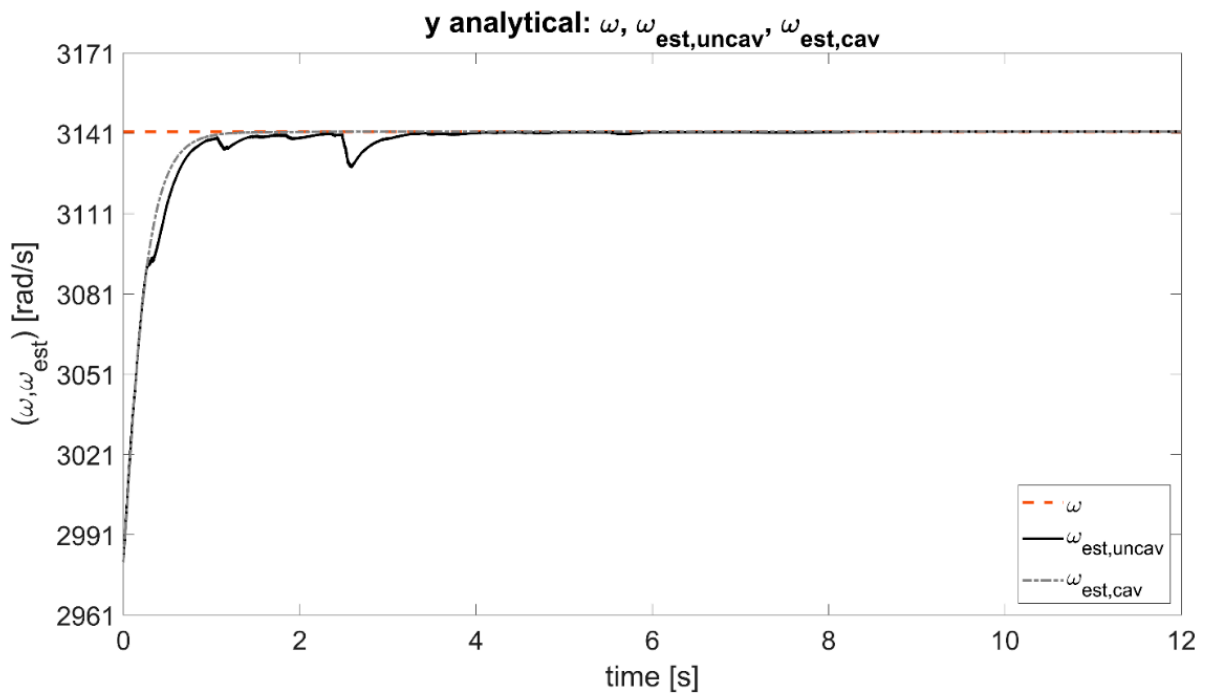


Figure 6. Comparison of frequency estimation performance in uncavitated and cavitated conditions with the analytical output noise  $y_{an}$ .

Figure 7 shows the comparison (in offset view) of phase estimation performance in time, in the four simulation cases. The  $(\hat{\varphi}_{unc,yan}, \hat{\varphi}_{unc,y})$  represent the phase estimate for the uncavitated case, with analytical and measured output noise, respectively; the  $(\hat{\varphi}_{cav,yan}, \hat{\varphi}_{cav,y})$  represent the phase estimate for the cavitated case, with analytical and measured output noise, respectively. In the graph, the warm-up phase edges, and time interval labels, are marked-up in the four cases for illustration purposes.

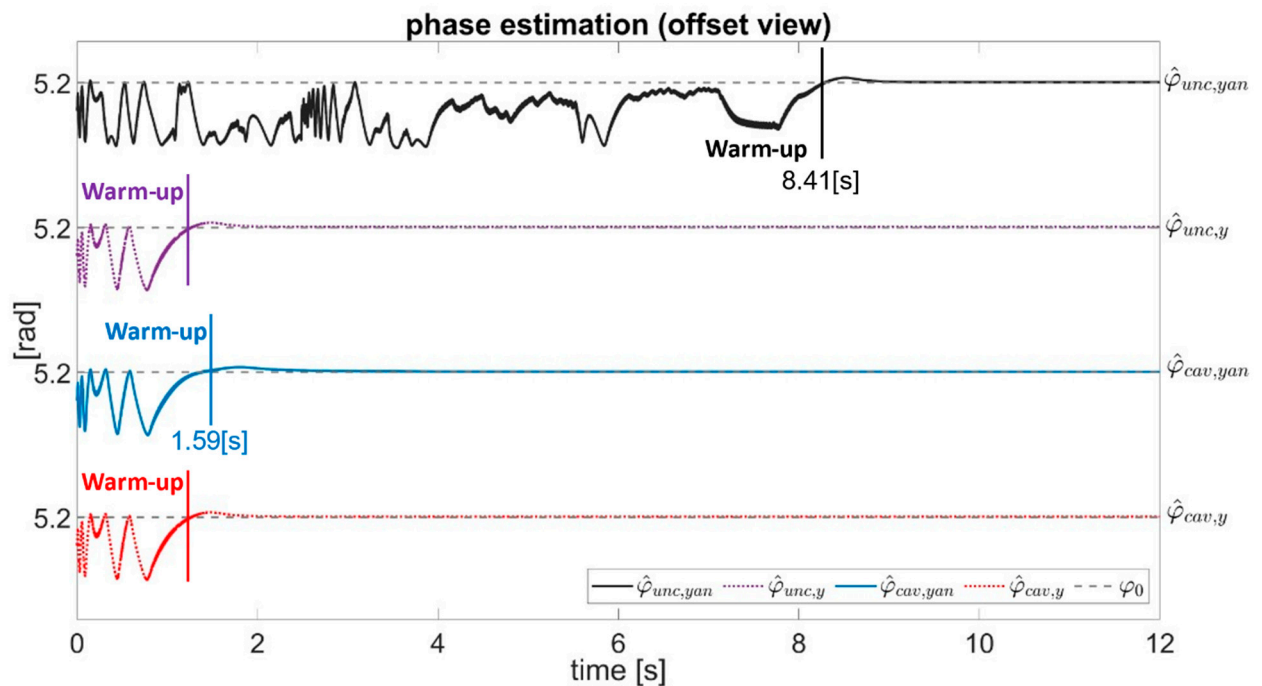
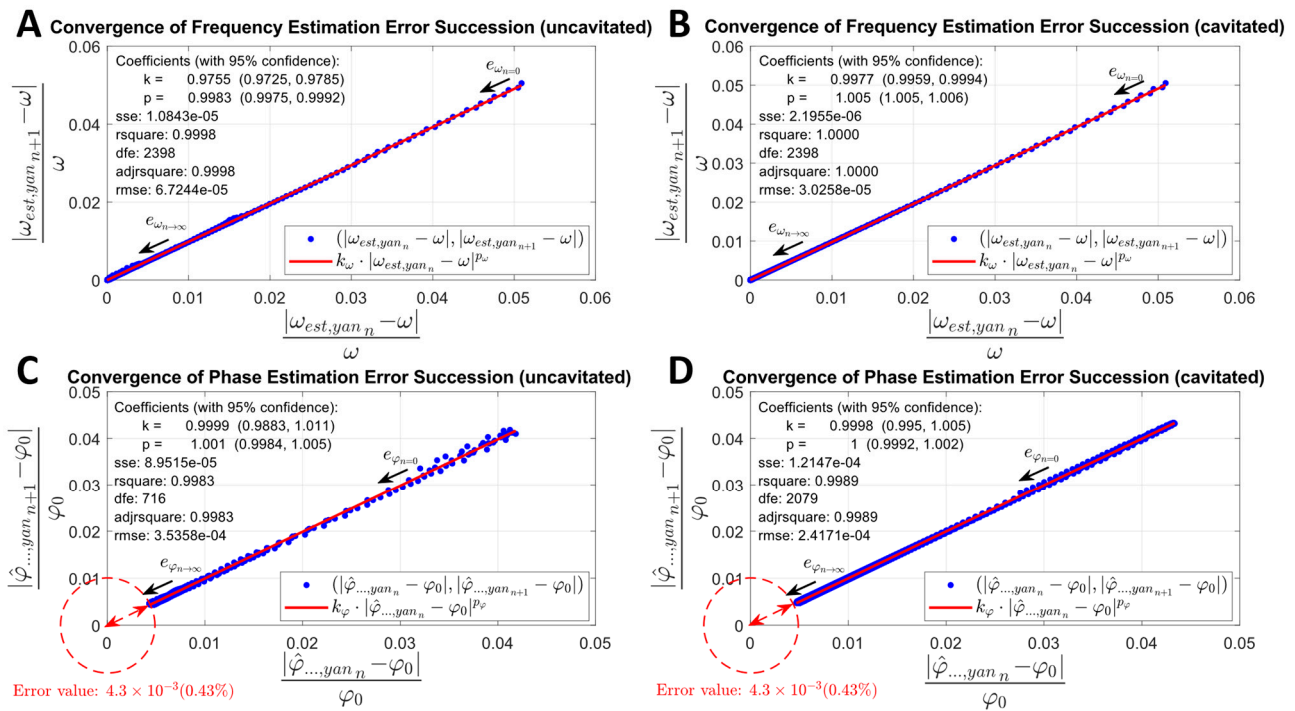


Figure 7. Offset view of phase estimation in the four simulation cases, with warm-up phase edges.

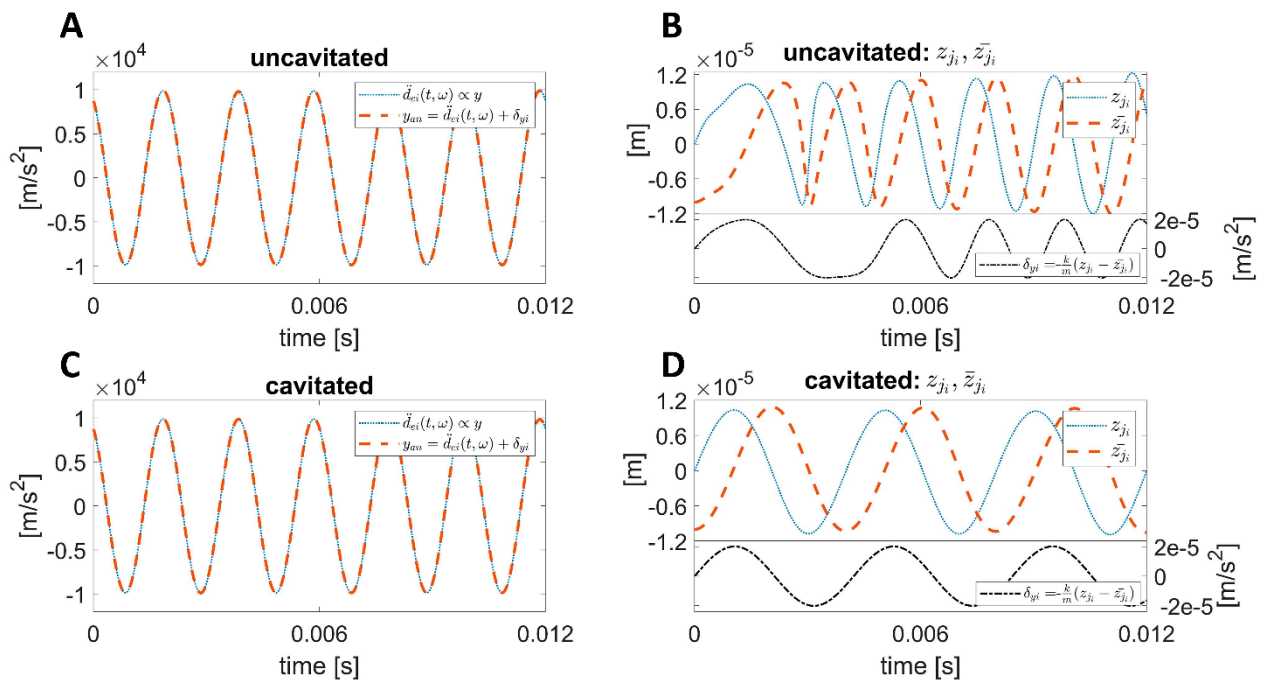
Figure 8 shows the scatter plot of the  $(k, p)$ -parametrized successions of frequency estimation error  $|e_{\omega_{n+1}}| = k_{\omega}|e_{\omega_n}|^{p_{\omega}}$  (Figure 8A,B) and phase estimation error  $|e_{\varphi_{n+1}}| = k_{\varphi}|e_{\varphi_n}|^{p_{\varphi}}$  (Figure 8C,D), following Equations (31)–(33). Both cavitated and uncavitated conditions with analytical output noise  $y_{an}$  are considered. The timeseries in Figure 8A,B are plotted considering the overall simulation time data. To evaluate whether the phase estimates' convergent behavior is exponential starting from the warm-up phase end (according to Proposition 1), the timeseries in Figure 8C,D are plotted on the two restricted simulation time intervals starting from 8.41 (s) and 1.59 (s) for uncavitated and cavitated cases, respectively, as shown in Figure 7.

The text boxes in Figure 8 report the fitting data statistics obtained applying the iterative Inexact Newton method on the frequency and phase estimation error timeseries, in cavitated and uncavitated conditions with analytical output noise. Such statistics are used to evaluate the order of the convergence  $p_{\omega,\varphi}$  in the four cases. The arrows indicate the direction of the succession point distribution from  $e_{\omega_{n=0}}$  to  $e_{\omega_{n \rightarrow \infty}}$ , and from  $e_{\varphi_{n=0}}$  to  $e_{\varphi_{n \rightarrow \infty}}$ , as defined in Equation (31).

Figure 9 shows the difference between the scalar analytical noise  $y_{an}$  and the actual disturbance component  $\ddot{d}_{ei}(t, \omega)$  for the uncavitated case (Figure 9A) and for the cavitated case (Figure 9C). For ease of graph interpretation, due to the high frequency of the signals, a restricted time lapse (0–0.0012) (s) was chosen, arbitrarily, on the overall simulation time of 12 (s), in order to highlight the detail of the comparison over a few periods.



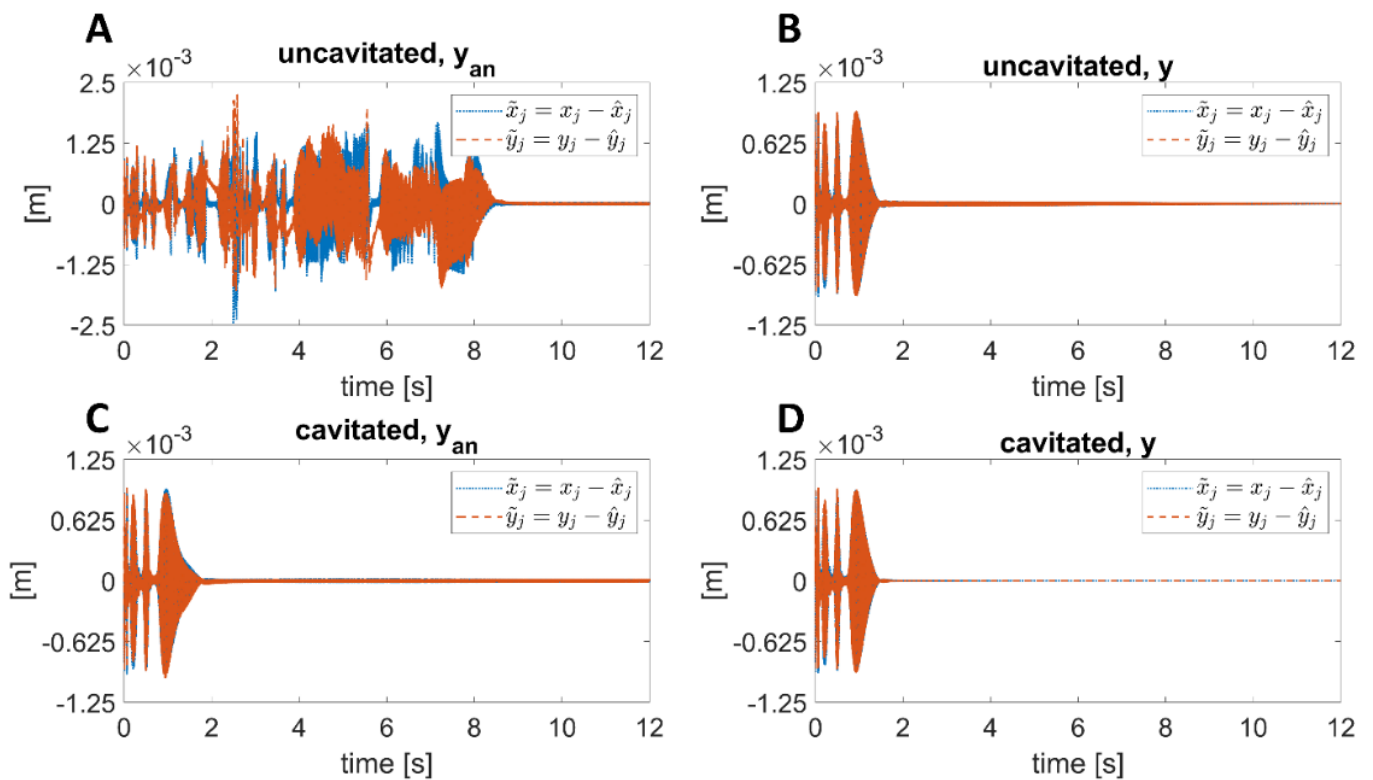
**Figure 8.** Convergence of frequency estimation error timeseries (A,B) and phase estimation error timeseries (C,D) for uncavitated and cavitated condition, with analytical output noise.



**Figure 9.** Scalar analytical output noise  $y_{an}$  and actual disturbance component  $\ddot{d}_{ei}(t, \omega)$  for uncavitated and cavitated conditions (A,C); “i” component of actual journal displacement  $z_{ji}$  and its analytically reconstruction  $\bar{z}_{ji}$  with the scaled difference  $\delta_{yi}$  for uncavitated and cavitated conditions (B,D).

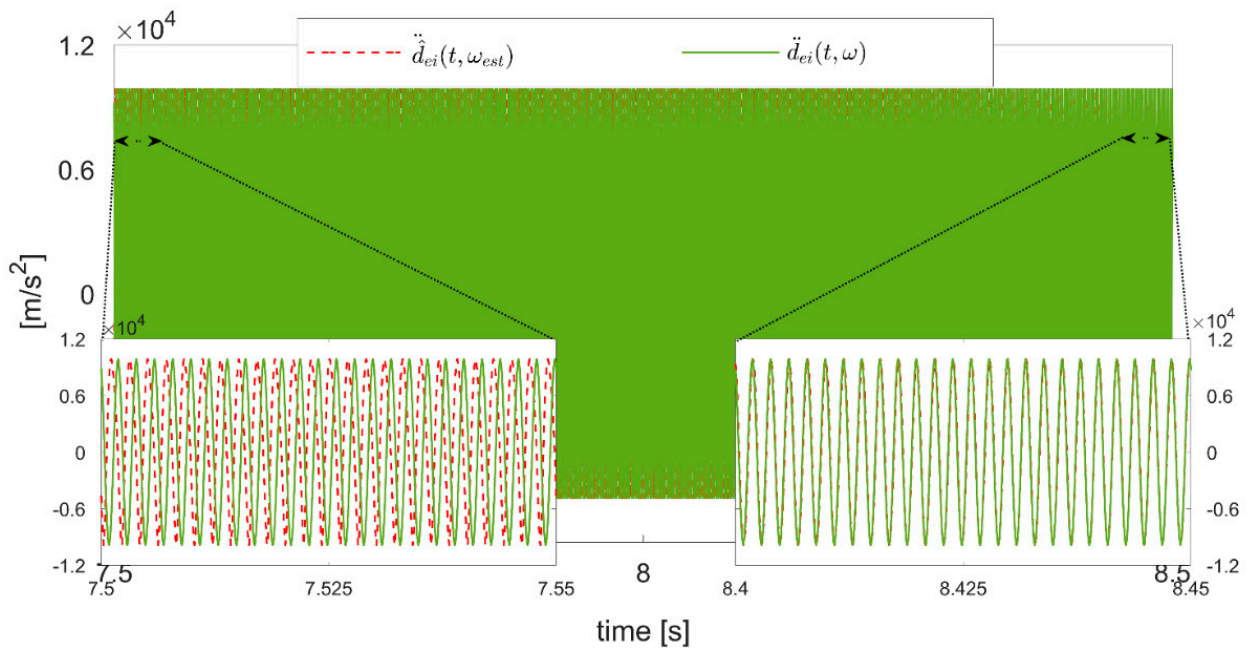
In Figure 9B,D, the behavior of only one component of the journal displacement coordinate vector,  $z_{ji}$ , is shown in time. It is compared with the same component “ $i$ ” of its analytically reconstructed value  $\bar{z}_{ji}$ . Both Figure 9B,D contain a subplot showing the scaled difference  $\delta_{yi} = -\frac{k}{m}(z_{ji} - \bar{z}_{ji})$ , where  $\delta_{yi}$  is the acceleration injected error referred to as only one component of the vector  $\delta_y(t, \bar{z}_{j0}, \omega, \hat{\omega}(t))$ , as defined in Equation (18).

Figure 10 shows the journal displacement observation errors  $\tilde{z}_j$  as defined according to Equations (20c) and (28), in the four simulation cases. The signals  $z_j = [x_j, y_j]^T$  are not available in practice, but they are shown only for comparison to their corresponding observation  $\hat{z}_j = [\hat{x}_j, \hat{y}_j]^T$ .



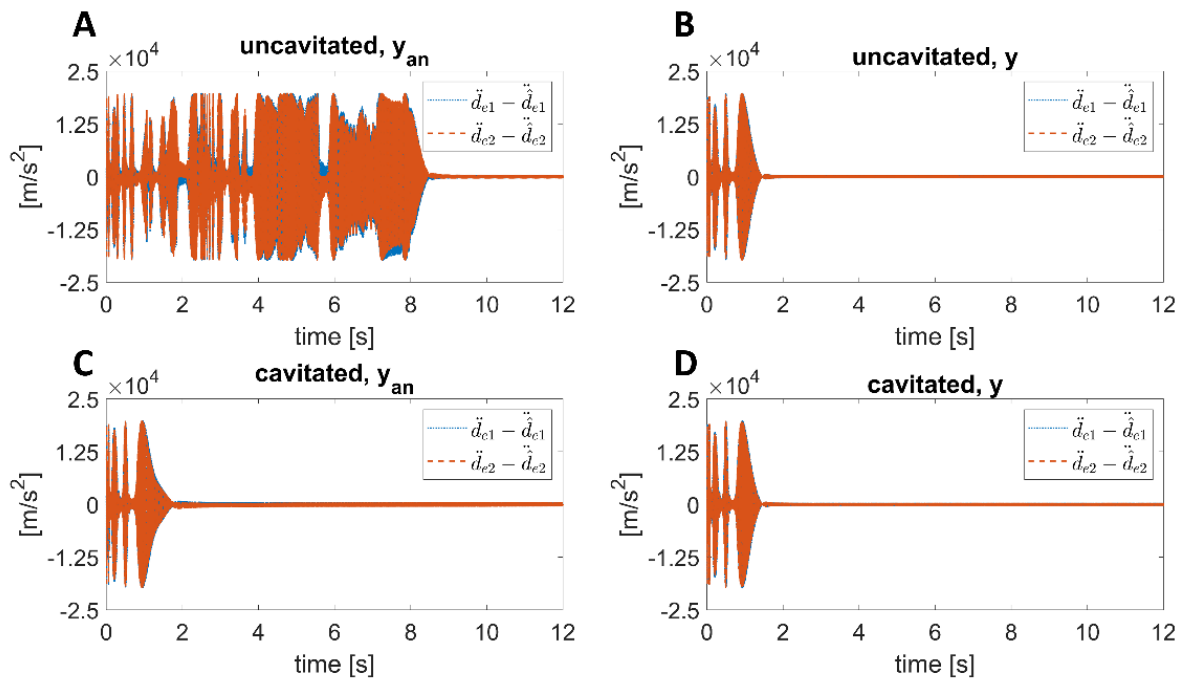
**Figure 10.** Observation errors of the journal displacement coordinate  $\tilde{z}_j$  with analytical output noise for uncavitated and cavitated conditions (A,C) and with measured output noise for uncavitated and cavitated conditions (B,D).

Figure 11 illustrates the hooking of the sinusoidal disturbance  $\ddot{d}_{ei}(t, \omega)$  by the estimate  $\ddot{\hat{d}}_{ei}(t, \omega_{est})$  in the case of the uncavitated condition with analytical noise. For ease of graph interpretation, due to the high frequency of the signals, the signal hooking is shown on the restricted time interval (7.5–8.5) (s).



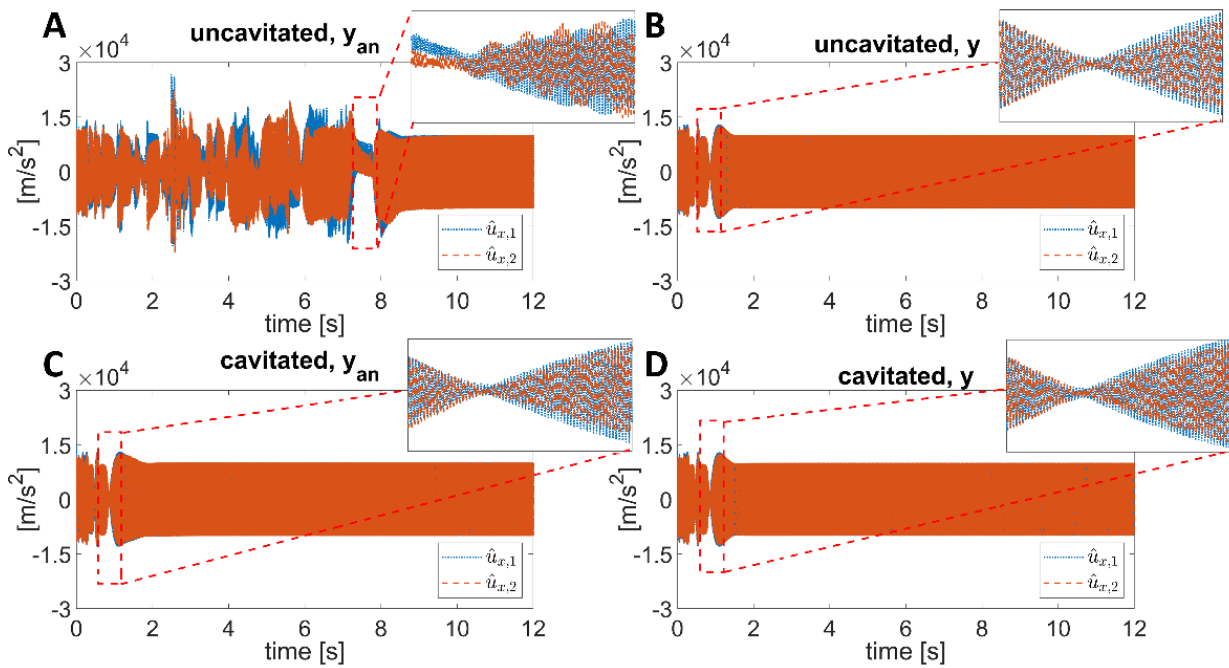
**Figure 11.** Hooking of the sinusoidal disturbance  $\ddot{d}_{ei}(t, \omega)$  by its estimate  $\hat{\ddot{d}}_{ei}(t, \omega_{est})$  in the case of uncavitated condition with analytical disturbance ( $y_{an}$ ).

Figure 12 illustrates the sinusoidal disturbance estimation errors  $\tilde{\ddot{d}}_{ei}(t, \omega)$  in the four simulation cases.



**Figure 12.** Sinusoidal disturbance estimation errors  $\tilde{\ddot{d}}_{ei}(t, \omega)$  are reported for uncavitated and cavitated conditions with analytical output noise (A,C) and for uncavitated and cavitated conditions with measured output noise (B,D).

In Figure 13, the control vector  $\hat{u}_x = [\hat{u}_{x,1}, \hat{u}_{x,2}]^T$  (Equation (20a)) is plotted in the four simulation cases. A zoomed plot, referred to by the dashed rectangle, highlights the detail of the last transient variation in the control before the steady-state behavior.



**Figure 13.** Control vector  $\hat{u}_x = [\hat{u}_{x,1}, \hat{u}_{x,2}]^T$  for uncavitated and cavitated conditions with analytical output noise (A,C) and for uncavitated and cavitated conditions with measured output noise (B,D).

Figure 14 illustrates the disturbance attenuation on disc center coordinates  $[x_c, y_c]$  in the four simulation cases.

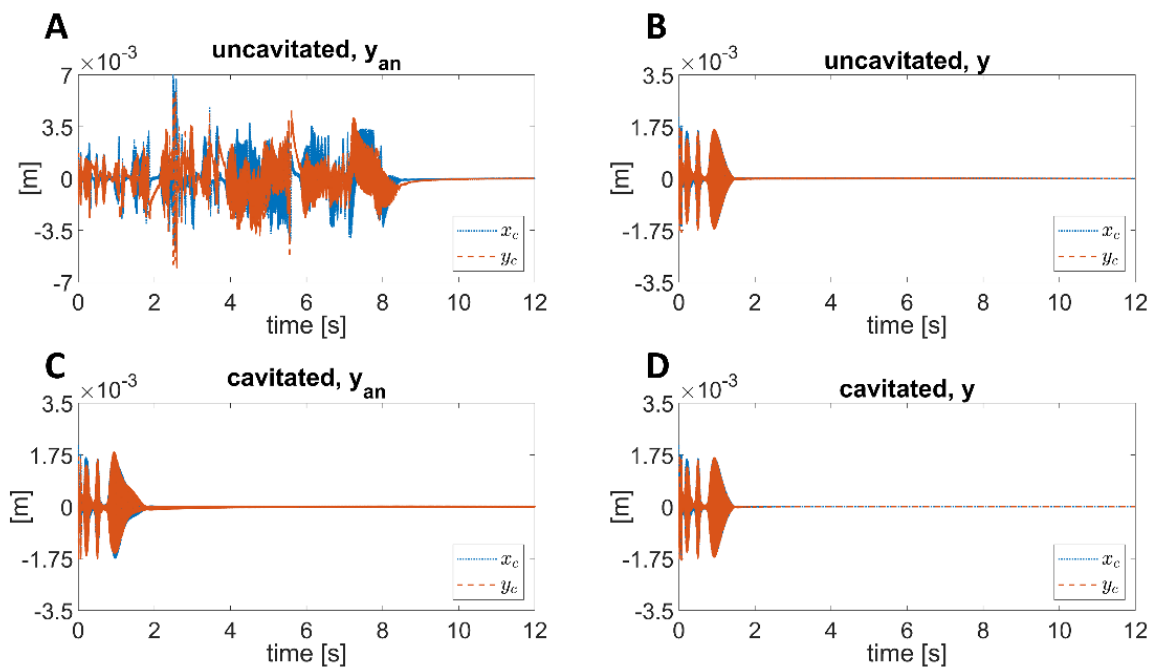


**Figure 14.** Disturbance attenuation of disc center coordinates  $(x_c, y_c)$  for uncavitated and cavitated conditions with analytical output noise (A,C) and for uncavitated and cavitated conditions with measured output noise (B,D).

## 5. Discussions and Conclusions

### 5.1. Discussions

The closed-loop ANC-FE operates on the output noise data to compute the asymptotical frequency estimate. In the following simulative analysis, both measured and analytical noise reconstruction is considered (in two cavitated and uncavitated operating conditions). Due to the reconstruction error  $\delta_y$  (Figure 9), the analytical output noise is affected by an intrinsic additive disturbance, which entails a data quality lowering with respect to the measured output noise case. The latter is considered an ideal case, and it is used in this analysis only for the sake of comparison.

The control performance, in terms of settling time, is evaluated in four simulation cases. From Figure 4 it emerges that, from the comparison between the case of analytical output noise  $\omega_{est,yan}$  and the case of measured output noise  $\omega_{est,y}$ , for the cavitated operating condition, the frequency estimation performance is very close. The residual vibration in the analytical case is due to the discrepancy between  $y$  and  $y_{an}$ , but it has a very low amplitude so that, macroscopically, the two curves cannot be distinguished. The comparison of the frequency estimation for the uncavitated condition is presented in Figure 5, showing that the performance degradation in terms of the settling of time, for analytical output noise  $\omega_{est,yan}$  with respect to measured output noise  $\omega_{est,y}$ , is restrained in 2 s. In Figure 6, both curves refer to the analytical output noise, and it is visible that different convergence performances are registered in cavitated and uncavitated cases. This difference is also recovered by the performance in phase estimation (Figure 7). As expected, the frequency estimation procedure represents a warm-up phase of the overall closed-loop disturbance estimation. In fact, according to Remark 6, the convergence of the asymptotical frequency estimate is standalone with respect to the rest of the control loop. Hence, only once the frequency estimate has reached its steady-state value, the phase estimation starts its exponential convergence ((thesis iii) of Proposition 1) in the last segment of all four curves (Figures 4, 5 and 7). The worst performance is registered in the uncavitated condition with analytical noise (solid black line in Figure 7) since the phase estimation settling time exceeds the other three simulation cases by 6 s.

The numerical analysis of the frequency and phase estimation timeseries gives the fitting results shown in Figure 8, considering 95% confidence in the goodness of fit (GOF) statistics. The order of convergence calculated for the frequency estimation timeseries are  $p_{\omega,unc} = 0.9983$  and  $p_{\omega,cav} = 1.005$  under uncavitated and cavitated conditions, respectively (Figure 8A,B), with acceptable GOF where the  $R_{\omega,unc}^2 = 0.9998$  and  $R_{\omega,cav}^2 = 1.0$ . The frequency estimation timeseries are sampled in the overall simulation time (degree of freedom,  $dfe = 2398$ ). Aiming to show that the phase estimation converges exponentially only after the initial warm-up (according to Proposition 1), in the case of phase estimation (Figure 8C,D), each timeseries sampling is restricted to the interval in which its own warm-up phase ends: 8.41 (s) ( $dfe = 716$ ) and 1.59 (s) ( $dfe = 2079$ ) under uncavitated and cavitated conditions, respectively, as shown in Figure 7. The convergence of phase estimation approximates the exponential behavior better than frequency estimation, obtaining  $p_{\phi,unc} = 1.001$  and  $p_{\phi,cav} = 1$  under uncavitated and cavitated conditions, respectively (Figure 8C,D) with acceptable GOF where  $R_{\phi,unc}^2 = 0.9983$  and  $R_{\phi,cav}^2 = 0.9989$ . The final phase estimation error is registered within 0.43%. Overall, with respect to the fitting curve, both frequency and phase estimation error timeseries exhibit less dispersion of the points in the cavitated case than the points sampled in the uncavitated condition.

Figure 9 illustrates that, although an additive disturbance  $\delta_{y_i}$  affects the analytical output  $y_{an}$ , due to the disturbance  $\delta_{y_i}$  amplitude, which is bounded and considerably smaller than the output noise itself (nine orders of magnitude less),  $y_{an}$  fits the real disturbance  $\ddot{d}_{ei}(t, \omega)$  very well in both cavitated and uncavitated conditions (Figure 9A,C). This enforces Assumption 1, and Proposition 1 applies. Figure 10 illustrates the comparison of the reduced-order observer performance (Equation (20c)) in the center journal coordinates' estimation in the four simulation cases. It emerges that the performance degradation in the journal vibration absorption in the two cases with the analytical output (Figure 10A,C)

is restrained in a few tenths of millimeters with respect to the ideal case with measured output (Figure 10B,D). The exponential hooking of the disturbance  $\ddot{d}_{ei}(t, \omega)$  by the adaptive noise cancellation control  $\hat{\ddot{d}}_{ei}(t, \omega_{est})$  (Equation (20b)) is illustrated in Figure 11. For sake of brevity, only the worst case (uncavitated condition with analytical output noise) is reported. Analogous results are obtained in the other three simulation cases. The preliminary phase of the overall disturbance estimations is dictated by the asymptotical convergence of the frequency estimate  $\omega_{est}$ . From that instant, the same closed-loop behavior of [24] is recovered, with the last segment of the disturbance convergence, which is exponential. The disturbance adaptation error  $\tilde{\ddot{d}}_{ei}(t, \omega)$ , reported in Figure 12, in the four cases recovers the observer behavior (Figure 10). Moreover, the behavior and performance of the control input (Figure 13) recover the behaviors of the displacement observation error (Figure 10) and the sinusoidal estimation errors (Figure 11) in the four cases. A zoomed plot is reported to highlight the sinusoidal trend of the two control vector components, oscillating at the same frequency as the rejected disturbance (as shown also in [24]). Figure 13 shows that the control amplitude stabilizes at the same time (respectively, in the four cases) in which all the estimation errors converge. Figure 14 illustrates that, from the comparison of the rotor center coordinate stabilization in the four cases, it emerges that the performance degradation in terms of vibration amplitude, for analytical output noise with respect to the (ideal) measured output noise case, is restrained in a few tenths of millimeters.

Overall, better estimation performance is obtained in the cavitated condition with respect to the uncavitated case. As the main figures of merit for the proposed adaptive closed-loop control, the rotor vibration attenuation time (about 8.5 (s) in the worst case) and the vibration residual amplitude (order of  $10^{-1}$  (mm)) are considered, which are acceptable values for a practical application. Similar results, in terms of estimation error convergence time, are obtained in [17,18] (order of seconds), which presented tests of an experimental setup on thin steel strips [17] (order of millimeters) and simulative *in silico* validation on a reversible cold strip rolling mill [18].

## 5.2. Conclusions

The aim of this study was to provide a mathematical model for a novel adaptive noise cancellation (ANC) technique designed to stabilize a flexible rotor shaft supported by two hydrodynamic full (short) journal bearings and affected by a sinusoidal disturbance output noise with unknown frequency. The disturbance frequency corresponds to the rotor operating angular speed ( $\omega$ ), which is driven by an external actuator, so that uncertainties may arise in the frequency actual value due to actuation operating point fluctuations. The adaptation with respect to the frequency estimation (FE) generalizes the ANC to the novel ANC-FE.

As the main novelty in this study, inspired from immersion and invariance (I&I) techniques, an asymptotical frequency estimation (FE) module is designed as a combination of state-observer and asymptotical parameter estimation. The FE operation represents the warm-up phase of the overall adaptive noise cancellation control. The FE module is externalized as an additive plug-in block, which processes the analytical reconstruction of the output data downstream of the ANC closed-loop system (Figure 2).

The mathematical structural proof of the ANC-FE control theoretical formulation, Proposition 1, is provided under Assumption 1, which requires that the analytical output noise reconstruction is a signal at the same frequency of disturbance. It follows that: the frequency estimation convergence is asymptotical; the disturbance phase estimation and the rotor center coordinate stabilization are exponential.

The mathematical results have been validated experimentally *in silico* by numerical simulations performed in four scenarios: cavitated and uncavitated conditions with analytical and measured output noise. Moreover, a data fitting analysis with the Inexact Newton method (with 95% of confidence) is performed on frequency and phase estimation error point series, in order to also validate numerically Proposition 1, demonstrating that the

phase estimate succession approximates the exponential behavior better than frequency estimate succession. The orders of convergence obtained by the frequency estimation timeseries are  $p_{\omega,unc} = 0.9983$  and  $p_{\omega,cav} = 1.005$ ; the order of convergence obtained by the phase estimation timeseries is  $p_{\varphi} = 1$  for both uncavitated and cavitated conditions. Considering the analytical output noise as the case of practical interest, the settling time of disturbance rejection and then of the rotor center coordinates stabilization is about 76% less in the cavitated than in the uncavitated condition, 2 (s) and 8.5 (s), respectively.

Simulation shows that the analytical output noise is very close to the measured output noise, enforcing Assumption 1. The warm-up phase length is restrained in less than 10 s, which is acceptable as an initialization process duration in a real application. For future investigations the possible application of the proposed control technique to other dynamical complex systems can be considered.

**Author Contributions:** Conceptualization, G.A., R.D. and A.R.; methodology, G.A. and R.D.; software, G.A.; validation, G.A. and R.D.; formal analysis, G.A., R.D. and A.R.; investigation, G.A., R.D. and A.R.; data curation, G.A.; writing—original draft preparation, G.A. and R.D.; writing—review and editing, G.A., R.D. and A.R.; visualization, G.A. and R.D.; supervision, A.R. All authors have read and agreed to the published version of the manuscript.

**Funding:** This research is funded by FARB 2019 University of Salerno (Italy).

**Institutional Review Board Statement:** Not applicable.

**Informed Consent Statement:** Not applicable.

**Conflicts of Interest:** The authors declare no conflict of interest.

## References

1. Friswell, M.I.; Penny, J.E.T.; Garvey, S.D.; Lees, A.W. *Dynamics of Rotating Machines*; Cambridge University Press: Cambridge, UK, 2010; ISBN 9780511780509.
2. Lund, J.W. Review of the Concept of Dynamic Coefficients for Fluid Film Journal Bearings. *J. Tribol. ASME US* **1987**, *109*, 37–41. [[CrossRef](#)]
3. Hamrock, B.J.; Schmid, S.R. *Fundamental of Fluid Film Lubrication*, 2nd ed.; CRC Press: Boca Raton, FL, USA, 2004; ISBN 0824753712.
4. Salazar, J.G.; Santos, I.F. Active tilting-pad journal bearings supporting flexible rotors: Part I—The hybrid lubrication. *Tribol. Int.* **2017**, *107*, 94–105. [[CrossRef](#)]
5. Chen, Y.; Yang, R.; Sugita, N.; Mao, J.; Shinshi, T. Identification of bearing dynamic parameters and unbalanced forces in a flexible rotor system supported by oil-film bearings and active magnetic devices. *Actuators* **2021**, *10*, 216. [[CrossRef](#)]
6. Muszynska, A. Stability of whirl and whip in rotor/bearing systems. *J. Sound Vib.* **1988**, *127*, 49–64. [[CrossRef](#)]
7. D’Agostino, V.; Guida, D.; Ruggiero, A.; Senatore, A. An analytical study of the fluid film force in finite-length journal bearings. Part I. *Lubr. Sci.* **2001**, *13*, 329–340. [[CrossRef](#)]
8. Poritsky, H. Contribution to the theory of oil whip. *Trans. ASME* **1953**, *75*, 1153–1161.
9. Tripathy, D.; Bhattacharyya, K. Analysis of a Hydrodynamic Journal Bearing of Circular Cross Section Lubricated by a Magnetomicropolar Fluid. In *Proceedings of the Lecture Notes in Mechanical Engineering*; Springer: Singapore, 2022; pp. 1495–1502.
10. Das, S.; Guha, S.K. Non-linear stability analysis of micropolar fluid lubricated journal bearings with turbulent effect. *Ind. Lubr. Tribol.* **2019**, *71*, 31–39. [[CrossRef](#)]
11. Bhattacharjee, B.; Chakraborti, P.; Choudhuri, K. Evaluation of the performance characteristics of double-layered porous micropolar fluid lubricated journal bearing. *Tribol. Int.* **2019**, *138*, 415–423. [[CrossRef](#)]
12. Harika, E.; Bouyer, J.; Fillon, M.; Hélène, M. Measurements of lubrication characteristics of a tilting pad thrust bearing disturbed by a water-contaminated lubricant. *Proc. Inst. Mech. Eng. Part J. J. Eng. Tribol.* **2013**, *227*, 16–25. [[CrossRef](#)]
13. Vania, A.; Pennacchi, P.; Chatterton, S. Dynamic Effects Caused by the Non-Linear Behavior of Oil-Film Journal Bearings in Rotating Machines. In *Proceedings of the Volume 7: Structures and Dynamics, Parts A and B*; ASME: New York, NY, USA, 2012; p. 657.
14. Das, S.; Guha, S.K.; Chattopadhyay, A.K. Linear stability analysis of hydrodynamic journal bearings under micropolar lubrication. *Tribol. Int.* **2005**, *38*, 500–507. [[CrossRef](#)]
15. Sukumaran Nair, V.P.; Prabhakaran Nair, K. Finite element analysis of elastohydrodynamic circular journal bearing with micropolar lubricants. *Finite Elem. Anal. Des.* **2004**, *41*, 75–89. [[CrossRef](#)]
16. Prabhakaran Nair, K.; Sukumaran Nair, V.P.; Jayadas, N.H. Static and dynamic analysis of elastohydrodynamic elliptical journal bearing with micropolar lubricant. *Tribol. Int.* **2007**, *40*, 297–305. [[CrossRef](#)]
17. Marko, L.; Saxinger, M.; Steinboeck, A.; Kugi, A. Cancellation of unknown multi-harmonic disturbances in multivariable flexible mechanical structures. *Automatica* **2022**, *137*, 110123. [[CrossRef](#)]

18. Liu, L.; Shao, N.; Deng, R.; Ding, S. Immersion and invariance adaptive decentralized control for the speed and tension system of the reversible cold strip rolling mill. *Int. J. Adapt. Control Signal Process.* **2022**, *36*, 785–801. [[CrossRef](#)]
19. Burrows, C.R.; Sahinkaya, M.N. Vibration control of multi-mode rotor-bearing systems. *Proc. R. Soc. Lond. A* **1983**, *386*, 77–94.
20. Ruggiero, A.; D'Amato, R.; Magliano, E.; Kozak, D. Dynamical simulations of a flexible rotor in cylindrical uncavitated and cavitated lubricated journal bearings. *Lubricants* **2018**, *6*, 40. [[CrossRef](#)]
21. Zhou, S.; Shi, J. Active balancing and vibration control of rotating machinery: A survey. *Shock Vib. Dig.* **2001**, *33*, 361–371. [[CrossRef](#)]
22. Stanway, R.; Burrows, C.R. Active vibration control of a flexible rotor on flexibly-mounted journal bearings. *J. Dyn. Syst. Meas. Control* **1981**, *103*, 383–388. [[CrossRef](#)]
23. Zheng, S.; Li, H.; Peng, C.; Wang, Y. Experimental Investigations of Resonance Vibration Control for Noncollocated AMB Flexible Rotor Systems. *IEEE Trans. Ind. Electron.* **2017**, *64*, 2226–2235. [[CrossRef](#)]
24. D'Amato, R.; Amato, G.; Wang, C.; Ruggiero, A. A Novel Tracking Control Strategy with Adaptive Noise Cancellation for Flexible Rotor Trajectories in Lubricated Bearings. *IEEE ASME Trans. Mechatron.* **2022**, *27*, 753–765. [[CrossRef](#)]
25. Lei, S.; Palazzolo, A. Control of flexible rotor systems with active magnetic bearings. *J. Sound Vib.* **2008**, *314*, 19–38. [[CrossRef](#)]
26. Marko, L.; Saxinger, M.; Steinboeck, A.; Kemmetmüller, W.; Kugi, A. Frequency-adaptive cancellation of harmonic disturbances at non-measurable positions of steel strips. *Mechatronics* **2020**, *71*, 102423. [[CrossRef](#)]
27. Marino, R.; Tomei, P. Adaptive disturbance rejection for unknown stable linear systems. *Trans. Inst. Meas. Control* **2016**, *38*, 640–647. [[CrossRef](#)]
28. Kumar, P.; Tiwari, R. Dynamic analysis and identification of unbalance and misalignment in a rigid rotor with two offset discs levitated by active magnetic bearings: A novel trial misalignment approach. *Propuls. Power Res.* **2020**, *10*, 58–82. [[CrossRef](#)]
29. D'Amato, R.; Amato, G.; Ruggiero, A. Adaptive Noise Cancellation-Based Tracking Control for a Flexible Rotor in Lubricated Journal Bearings. In Proceedings of the 2019 23rd International Conference on Mechatronics Technology (ICMT), Salerno, Italy, 23–26 October 2019; pp. 1–5. [[CrossRef](#)]
30. Vance, J.M. *Rotordynamics of Turbomachinery*; Wiley: Hoboken, NJ, USA, 1988; ISBN 0471802581.
31. Avramov, K.V.; Borysiuk, O.V. Nonlinear dynamics of one disk asymmetrical rotor supported by two journal bearings. *Nonlinear Dyn.* **2012**, *67*, 1201–1219. [[CrossRef](#)]
32. Carnevale, D.; Astolfi, A. A minimal dimension observer for global frequency estimation. *Proc. Am. Control Conf.* **2008**, *2*, 5236–5241. [[CrossRef](#)]
33. Carnevale, D. Robust hybrid estimation and rejection of multi-frequency signals. *Int. J. Adapt. Control Signal Process.* **2016**, *30*, 1649–1673. [[CrossRef](#)]
34. Hoad, K.; Robinson, S.; Davies, R. Automating warm-up length estimation. *J. Oper. Res. Soc.* **2010**, *61*, 1389–1403. [[CrossRef](#)]
35. Ballnus, B.; Schaper, S.; Theis, F.J.; Hasenauer, J. Bayesian parameter estimation for biochemical reaction networks using region-based adaptive parallel tempering. *Bioinformatics* **2018**, *34*, i494–i501. [[CrossRef](#)]
36. Ypma, T.J. Local Convergence of Inexact Newton Methods. *SIAM J. Numer. Anal.* **2006**, *21*, 583–590. [[CrossRef](#)]
37. Sastry, S.; Bodson, M. *Adaptive Control—Stability, Convergence, and Robustness*; Prentice-Hall: Hoboken, NJ, USA, 1989; p. 201.
38. Marino, R.; Tomei, P. Output Regulation for Unknown Stable Linear Systems. *IEEE Trans. Autom. Control* **2015**, *60*, 2213–2218. [[CrossRef](#)]
39. Sun, X.; Member, S.; Wu, M.; Yin, C.; Wang, S.; Tian, X. Multiple-Iteration Search Sensorless Control for Linear Motor in Vehicle Regenerative Suspension. *IEEE Trans. Transp. Electrif.* **2021**, *7*, 1628–1637. [[CrossRef](#)]
40. Marino, R.; Tomei, P. *Nonlinear Control Design: Geometric, Adaptive and Robust*; Prentice Hall: London, UK, 1995; Volume 1.
41. Marino, R.; Tomei, P.; Verrelli, C.M. *Induction Motor Control Design*; Springer Science & Business Media: Berlin/Heidelberg, Germany, 2010; ISBN 1849962847.